

1 Laser-Driven, Ion-Scale Magnetospheres in Laboratory Plasmas. I.

2 Experimental Platform and First Results

3 D. B. Schaeffer,^{1,a)} F. D. Cruz,² R. S. Dorst,³ F. Cruz,² P. V. Heuer,³ C. G. Constantin,³ P. Pribyl,³ C.
4 Niemann,³ L. O. Silva,² and A. Bhattacharjee,¹

5 ¹⁾Department of Astrophysical Sciences, Princeton University, Princeton, NJ 08540,
6 USA

7 ²⁾GoLP/Instituto de Plasmas e Fusão Nuclear, Instituto Superior Técnico, Universidade de Lisboa, 1049-001 Lisboa,
8 Portugal

9 ³⁾Department of Physics and Astronomy, University of California – Los Angeles, Los Angeles, CA 90095,
10 USA

11 ⁴⁾Princeton Plasma Physics Laboratory, Princeton, NJ 08543, USA

12 (Dated: 22 February 2022)

Magnetospheres are a ubiquitous feature of magnetized bodies embedded in a plasma flow. While large planetary magnetospheres have been studied for decades by spacecraft, ion-scale “mini” magnetospheres can provide a unique environment to study kinetic-scale, collisionless plasma physics in the laboratory to help validate models of larger systems. In this work, we present preliminary experiments of ion-scale magnetospheres performed on a unique high-repetition-rate platform developed for the Large Plasma Device (LAPD) at UCLA. The experiments utilize a high-repetition-rate laser to drive a fast plasma flow into a pulsed dipole magnetic field embedded in a uniform magnetized background plasma. 2D maps of magnetic field with high spatial and temporal resolution are measured with magnetic flux probes to examine the evolution of magnetosphere and current density structures for a range of dipole and upstream parameters. The results are further compared to 2D PIC simulations to identify key observational signatures of the kinetic-scale structures and dynamics of the laser-driven plasma. We find that distinct 2D kinetic-scale magnetopause and diamagnetic current structures are formed at higher dipole moments, and their locations are consistent with predictions based on pressure balances and energy conservation.

13 I. INTRODUCTION

14 Magnetospheres form when a plasma flow impacts a magnetic obstacle, such as the interaction between the
15 solar wind and planets with intrinsic magnetic fields in
16 the heliosphere. The plasma flow is largely stopped at the
17 magnetopause, where the kinetic ram pressure of the flow
18 balances the magnetic field pressure, and moves around
19 the obstacle to form a magnetotail downstream. If the
20 incoming flow is super-Alfvénic, a bow shock can also be
21 created ahead of the magnetopause, leading to the genera-
22 tion of a magnetosheath composed of shocked plasma.
23 Additionally, if the magnetic obstacle is embedded in a
24 background magnetic field (analogous to the interplan-
25 etary magnetic field [IMF]), the orientation of the obsta-
26 cle relative to the background field can have significant
27 effects on the global magnetic structure, including mag-
28 netic reconnection. These features are readily observed
29 at planets, including the Earth, which has been studied
30 *in situ* by spacecraft for decades^{1–4}.

31 To first order, the magnetic obstacles of interest can be
32 modeled as dipoles, so that magnetospheres can be char-
33 acterized by the so-called Hall parameter $D = L_M/d_i$,
34 where L_M is the distance from the dipole center to the
35 magnetopause, and $d_i = c/\omega_{pi}$ is the upstream ion in-
36 erial length. In other words, D can be interpreted as

37 the effective size of the magnetic obstacle^{5,6}. Planetary
38 magnetospheres are large; indeed, for Earth $D > 600$. If
39 the magnetopause distance is comparable to the ion iner-
40 tial length, though, ion-scale magnetospheres can form.
41 These mini-magnetospheres have been observed in a vari-
42 ety of natural systems, including around comets⁷ and lo-
43 cally magnetized regions on the Moon^{8–12}, and are of in-
44 terest for spacecraft propulsion¹³. However, understand-
45 ing both their local and global scale structures (both
46 kinetic and system size) has been constrained by avail-
47 able spacecraft diagnostics and single-spacecraft trajec-
48 tories. These limitations have been partially addressed
49 by numerical efforts, where fully-kinetic^{14,15} and hybrid-
50 fluid-kinetic simulations^{16–19} have shown the importance
51 of expanding beyond MHD descriptions when modeling
52 magnetospheres, including mini-magnetospheres^{20–22}.

53 Laboratory experiments can thus help address key
54 questions about ion-scale magnetospheres and comple-
55 ment spacecraft and numerical efforts by providing con-
56 trolled and reproducible conditions and measurements of
57 both global and kinetic scales. 2D hybrid simulations (ki-
58 netic ions, fluid electrons)^{5,23–25} have shown that differ-
59 ent regimes of magnetosphere formation can be parame-
60 terized with D . The results indicate that for $D \ll 1$,
61 there is no appreciable flow deflection, though whistler
62 waves can develop in the obstacle's wake. At larger
63 $D \sim 1$, there is some pile-up of plasma at the magne-
64 topause, resulting in a fast mode bow wave and some
65 heating in the magnetotail. Only in the large-scale Hall
66 regime ($D > 20$) are fully formed magnetospheres, in-

^{a)}Electronic mail: dereks@princeton.edu

This is the author's peer reviewed, accepted manuscript. However, the online version of record will be different from this version once it has been copyedited and typeset.

PLEASE CITE THIS ARTICLE AS DOI: 10.1063/5.0084353

cluding the presence of a bow shock, observed. More recently, 3D fully kinetic particle-in-cell (PIC) simulations have shown that bow shocks can form when $L_M/\rho_i > 1$, where ρ_i is the upstream ion gyroradius²⁶. This condition is equivalent to $D > M_A$, where M_A is the Alfvénic Mach number of the plasma flow and $\rho_i = M_A d_i$. These simulations thus predict that for low Mach number flows, the conditions necessary to form a magnetosphere are less stringent than those suggested by the earlier hybrid simulations.

Following the development of these large-scale magnetospheric simulations, there has been increased interest in laboratory experiments over the past couple decades. Work by Yur *et al.*^{27,28} used a plasma gun to study the structure of the magnetotail and its dependence on the orientation of a background magnetic field. Utilizing a super-Alfvénic plasma flow and magnetic dipole, early experiments by Brady *et al.*²⁹ confirmed that the location of the flow-dipole pressure balance (L_M) could be modeled with MHD in the small Hall regime ($D \ll 1$). Bamford *et al.*¹¹ used a plasma wind tunnel to study similarly weak interactions relevant to lunar mini-magnetospheres. Experiments by Zakharov *et al.*³⁰, and later Shaikhislamov *et al.*^{6,31}, utilized a high-energy laser to drive a super-Alfvénic plasma flow into a magnetic dipole, and in several cases incorporated a theta pinch to provide an ambient plasma and external magnetic field. While these experiments achieved $D \sim 1 < M_A$, measurements were limited to 1D magnetic field and plasma density profiles.

To overcome these limitations, we have developed a new experimental platform to study ion-scale magnetospheres on the Large Plasma Device (LAPD) at UCLA. This platform uniquely combines the large-scale, ambient magnetized plasma provided by the LAPD, a fast collisionless plasma flow generated by a laser driver, and a rotatable pulsed dipole magnetic field, all operating at high-repetition-rate (~ 1 Hz). Utilizing motorized probes, we can measure for the first time the 3D structure of mini-magnetospheres over a wide range of parameters and magnetic geometries. The goals of these experiments are 1) to study the formation and structure of laser-driven ion-scale magnetospheres, 2) to study the effect of magnetic reconnection on magnetosphere dynamics, and 3) to utilize super-Alfvénic flows to generate and study bow shocks in the $D > M_A > 1$ regime.

In this paper, we report the first results from experiments on laser-driven, ion-scale magnetospheres on the LAPD that focus on the formation of magnetosphere structure with sub-Alfvénic flows. In the experiments, a laser-driven plasma expands supersonically into a dipole magnetic field embedded in an ambient magnetized plasma, so that the total magnetic field topology is analogous to that of the Earth's magnetosphere superposed with a northward IMF. By measuring 2D planes of the magnetic field over thousands of shots, we demonstrate the formation of a magnetopause and show how its structure evolves in time for a range of dipole strengths in the $D \sim 1$ regime. The results are consistent with 2D

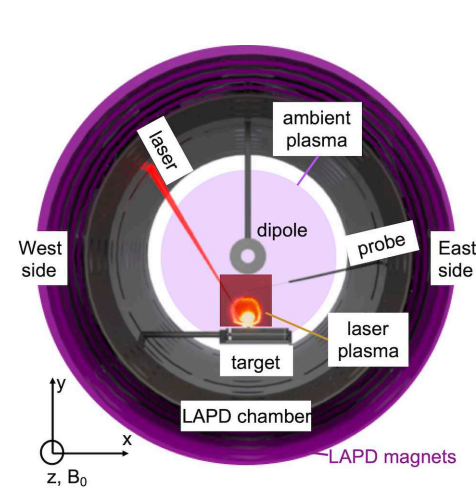


FIG. 1: Schematic of the experimental setup on the LAPD. A laser ablates a plastic target to create a supersonic plasma flow, which flows towards a dipole magnet inserted into the LAPD from the top. The dipole magnet is embedded in a uniform magnetized background plasma generated by the LAPD. Probes inserted from the east port collect volumetric data from the regions around the dipole. A fast-gate image shows the expansion of the laser-driven plasma.

PIC simulations modeled after the experiments, which show that both the ambient and laser-produced ions play a key role in the formation of the magnetosphere. Additional simulation results are presented as the second part of this series³², hereafter referred to as Part II.

The paper is organized as follows. Section II describes the setup of the experiments and typical parameters. Section III discusses the main results, including: the performance of the dipole magnet, fast-gate images of the laser-driven plasma, measurements of the magnetosphere, and comparisons with simulations. The interpretation of the results are discussed in Sec. IV before concluding in Sec. V.

II. EXPERIMENTAL SETUP

The experiments were carried out on the Large Plasma Device (LAPD) at UCLA, operated by the Basic Plasma Science Facility (BaPSF), and combined a magnetized ambient plasma, a fast laser-driven plasma flow, and a current-driven dipole magnet. A schematic of the experimental setup is shown in Fig. 1, and typical background and laser-driven plasma parameters are listed in Table I. The LAPD³³ is a cylindrical vacuum vessel (20 m long by 1 m diameter) that can generate a steady-state (~ 15 ms), large volume (> 50 cm across the plasma column), magnetized ambient plasma at high repetition (up to 1 Hz). The machine can produce variable background magnetic

fields (200-1500 G), variable ambient gas fills (e.g. H, He), and variable ambient densities ($10^{11} - 10^{13} \text{ cm}^{-3}$). The ambient plasma is generated from the combination of two cathodes. A BaO-coated Ni cathode generates a $\varnothing 60 \text{ cm}$, lower-density ($n \sim 2 \times 10^{12} \text{ cm}^{-3}$) main plasma, while a LaB₆ (lanthanum hexaboride) cathode generates a smaller $\varnothing 20 \text{ cm}$, higher-density ($n \sim 2 \times 10^{13} \text{ cm}^{-3}$) core plasma roughly centered on the main one. The ambient plasma has a typical electron temperature $T_e \approx 5-10 \text{ eV}$ and ion temperature $T_i \approx 1 \text{ eV}$. The background field is oriented axially (\hat{z}) along the machine, with \hat{x} oriented horizontally perpendicular to the field and \hat{y} oriented vertically.

The supersonic plasma flow was generated by the high-repetition-rate Peening^{34,35} laser, operated by the UCLA High Energy Density Plasma (HEDP) group³⁶. The Peening laser (1053 nm) can deliver energies up to 20 J with a pulse width of 15 ns (FWHM), yielding typical intensities of 10^{12} W/cm^2 and repetition rates up to 4 Hz. The output laser energy, pulse shape, diffraction-limited focus, and beam pointing are stable to within 5%³⁵.

The dipole magnet consisted of an epoxy-covered 24-turn copper coil with integrated water cooling and a non-magnetic stainless steel housing and support shaft. It has a 14 cm outer diameter and a 4 cm inner diameter. A pulsed power cabinet was capable of driving up to 7 kA at 800 V through the coil, corresponding to peak on-axis magnetic fields of 15 kG (magnetic moment $M \approx 2.2 \text{ kAm}^2$, sufficient to achieve large standoff values), which is approximately constant for several tens of μs (i.e. the whole experiment). The field could be pulsed up to 1 Hz (1/4 Hz at the highest currents), and the water cooling allows the magnet to remain at room temperature throughout operation.

The target was a long, 5 cm diameter cylindrical rod of high-density polyethylene (C₂H₄) plastic. The target was mounted on a 2D stepper motor drive synchronized with the laser, which translated and rotated the target in a helical pattern. Each target position was repeated three times and then moved to provide a fresh surface. A single target could thus be used for up to 2×10^4 laser shots.

The dipole magnet was inserted from the top flange, so that the distance from the target to the dipole was variable, with the dipole orientation such that the dipole axis was along z and rotatable about the y axis. The lasers were timed to fire at the peak of the dipole field (time t_0), and the experiment lasted for a few tens μs , well within the long ($\sim 10 \text{ ms}$) lifetime of the ambient plasma. The target and probes were set up in a "dayside" configuration, analogous to the sun-facing region of Earth's magnetosphere, as follows. The target was inserted through the bottom 45° west-side port at an angle parallel to the bottom flange (i.e. along \hat{x}), which placed the target surface 27.5 cm from the chamber center. The laser was routed from the laserbay, through the LAPD room ceiling, to the top 45° west-side port, where it was focused and

sent through a vacuum window, impinging the target at an angle of 30° relative to the target surface normal. The resulting laser plasma expanded up towards the dipole, and probes were inserted from the east-side. This arrangement allowed probes to move throughout the dayside region of the magnetosphere. The laser, target, and pulsed dipole magnet were synchronized to the LAPD, and they all operated at a repetition rate of 1/4 Hz to allow time for the diagnostics to position themselves between shots.

During the experiments, the ambient gas fill was H and the background magnetic field was set to 300 G. The dipole magnet was arranged such that the dipole magnetic field was parallel to the background field in the dayside region. The laser ablated a highly-energetic supersonic plasma, consisting of both C and H ions from the target, that expanded towards the dipole and transverse to the background (LAPD) magnetic field. The interaction between the flowing and stationary ions is highly collisionless (mean free path \gg system size) due to the high flow speeds. The background electrons were also collisionless as the electron-ion collision time was much larger than the electron gyroperiod $\omega_{ce0}\tau_{ei} \approx 500$.

The magnetic field topology and dynamics were measured with 3 mm diameter, 3-axis 10-turn magnetic flux ("bdot") probes³⁷. The probe signals were passed through a 150 MHz differential amplifier and coupled to either fast (1.25 GHz) or slow (100 MHz) 10-bit digitizers, and then numerically integrated to yield magnetic field amplitude. To acquire data, the probes were positioned by a 3D motorized probe drive (resolution $< 0.1 \text{ cm}$)³⁸ in between shots. Datasets were compiled by moving the probes in small increments of 0.25 cm with 3 shots per position for statistics.

Fast-gate ($\sim 10 \text{ ns}$) imaging³⁹ was used to acquire 2D snapshots of plasma self-emission during the interaction of the laser-plasma and dipole using an intensified charge-coupled device (ICCD) camera. The camera viewed along the LAPD central axis through a mirror mounted inside of the LAPD chamber. Highly temporally-resolved movies were acquired over hundreds or thousands of shots by incrementing the camera delay relative to the laser trigger.

Additionally, swept Langmuir probes were employed to measure x - z and x - y planes of plasma electron density and temperature near the dipole magnet. These measurements were carried out in the absence of the laser plasma, and so provide the initial state of the ambient plasma at t_0 .

III. RESULTS

When measuring the interaction of the laser-driven plasma with the dipole magnetic field, the dipole field evolves too slowly ($\sim \text{ms}$) to be measured on the timescales ($\sim \mu\text{s}$) of the laser-driven plasma. Instead, the contributions to the total field from the laser-driven

	Run 1	Run 2	Run 3	Run 4	Run 5
Background Parameters					
Dipole magnetic moment M	0 Am ²	95 Am ²	475 Am ²	950 Am ²	950 Am ²
Ion species		H ⁺			
Density n_0		$\sim 3 \times 10^{12} \text{ cm}^{-3}$			0 cm ⁻³
Magnetic field B_0		300 G			0 G
Electron temperature T_{e0}		$\sim 5 \text{ eV}$			—
Electron inertial length d_{e0}		0.3 cm			—
Electron gyroperiod ω_{ce0}^{-1}		0.2 ns			—
Ion temperature T_{i0}		$\sim 1 \text{ eV}$			—
Ion inertial length d_{i0}		13.2 cm			—
Ion gyroperiod ω_{ci0}^{-1}		348 ns			—
Alfvén speed v_A		378 km/s			—
Laser-Driven Parameters					
Laser energy E_{laser}		20 J			
Plasma speed v_l		210 km/s			
Ion species		H ⁺ , C ⁺¹⁻⁶			
Electron gyroradius $\rho_e = v_l/\omega_{ce0}$		40 μm			—
H ion gyroradius $\rho_H = v_l/\omega_{ci0}$		7.3 cm			—
C ion gyroperiod $\omega_{ci0,C}^{-1}$		$(0.7 - 4.2) \times 10^3 \text{ ns}$			—
C ion gyroradius $\rho_C = v_l/\omega_{ci0,C}$		14.6 - 87.7 cm			—
Magnetic cavity speed v_0		135 km/s			165 km/s
Magnetic cavity standoff L_{dia}	11.5 cm	13.75 cm	15 cm	> 15.5 cm	12.25 cm
Magnetopause standoff L_M	—	< 9 cm	13 cm	> 15.5 cm	12.25 cm
Dimensionless Parameters					
Thermal $\beta = 8\pi n_0 T_{e0}/B_0^2$		0.01			—
Electron magnetization ρ_{e0}/d_{i0}		0.001			—
Ion magnetization ρ_{i0}/d_{i0}		0.02			—
Electron collisionality $\omega_{ce0} \tau_{ei}$		5×10^2			—
Mach number $M_s = v_l/v_s$		5.3			—
Alfvén Mach number $M_A = v_l/v_A$		0.6			—
Hall parameter $D = L_M/d_{i0}$	—	< 0.7	1	> 1.2	—

TABLE I: Summary of experimental runs with typical plasma parameters. For the laser-driven plasma, parameters are given for the range of C ionization between C⁺¹ and C⁺⁶. The magnetization for species s is calculated with respect to the background gyroradii $\rho_{s0} = v_{th,s}/\omega_{cs0}$, where $v_{th,s} \propto \sqrt{T_s/m_s}$.

plasma interaction and from the dipole magnet were measured in separate runs with the same bdot probe. Runs with the laser-driven plasma were digitized at 1.25 GHz over a few tens of μs to record the laser-plasma-dipole interaction. The same runs without the laser-driven plasma were then digitized at 100 MHz over several ms to cover a full period of the dipole-only field. The total field during the lifetime of the experiment is then calculated as $\mathbf{B}_{tot} = \Delta\mathbf{B} + \mathbf{B}_{init}$, where $\Delta\mathbf{B}$ is the field measured during the laser-plasma interaction, and $\mathbf{B}_{init} = \mathbf{B}_{dip} + \mathbf{B}_0$ is the initial unperturbed field due to the slowly-evolving dipole field \mathbf{B}_{dip} and the uniform background field $\mathbf{B}_0 = B_0 \hat{z}$.

A. Performance of Dipole Magnet

The performance of the dipole magnet is shown in Fig. 2(a)-(b) for a dipole coil current of 3 kA. For these measurements, the dipole magnet was embedded in the background field B_0 and background plasma, but there was no laser-driven plasma. While the dipole coil center is nominally located at the center of the LAPD cham-

ber ($\{x, y, z\} = \{0, 0, 0\}$), measurements indicate that it is slightly offset, with the peak field along y located at $x = 0.75 \text{ cm}$. At $y = -9 \text{ cm}$ (the closest to the magnet we can measure), the dipole reaches a peak value of $B_{z,dip} \approx 1500 \text{ G}$ in $\approx 685 \mu\text{s}$ and is constant in magnitude to within 1% for over 100 μs (longer than the lifetime of the experiment). Fig. 2(c) shows profiles of the total z-component of the magnetic field $B_{z,tot} = B_0 + B_{z,dip}$ along y at $x = 0.75 \text{ cm}$ for 3 kA (black), 1.5 kA (red), and 0.3 kA (green) dipole coil currents. Similar profiles along x at $y = 0$ are shown in Fig. 2(d). The profiles are well-modeled (dashed curves) by the far-field dipole approximation $B_{z,dip} = M/y^3$, where M is the magnetic moment and y is the distance from the dipole center. For a 3 kA dipole current, the magnetic moment $M_{950} \approx 950 \text{ Am}^2$. The moments scale linearly with the current, so that the 1.5 kA and 0.3 kA runs correspond to $M_{475} \approx 475 \text{ Am}^2$ and $M_{95} \approx 95 \text{ Am}^2$, respectively.

This is the author's peer reviewed, accepted manuscript. However, the online version of record will be different from this version once it has been copyedited and typeset.

PLEASE CITE THIS ARTICLE AS DOI: 10.1063/5.0084353

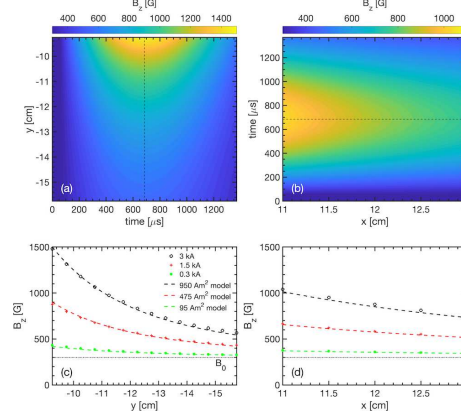


FIG. 2: Streak plots of the measured dipole magnetic field (a) along y at $x = 0.75$ cm and (b) along x at $y = 0$ cm for a 3 kA current. (c) Comparison of the total magnetic field profiles $B_{z,tot} = B_0 + B_{z,dip}$ at the time of peak field ($t \approx 685$ μ s) for 3 kA (black), 1.5 kA (red), and 0.3 kA (green) dipole currents. The field profiles are modeled using the far-field dipole approximation $B_{z,dip} = M/y^3$, where M is the magnetic moment. (d) Similar field profiles and models at the same time in (b).

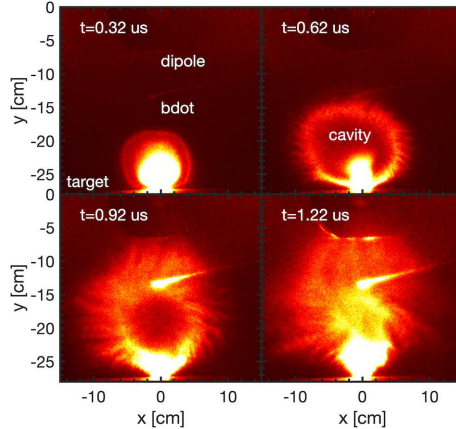


FIG. 3: Fast-gate images of plasma optical self-emission for a run with $M = 950$ Am 2 . Each image is gated over 10 ns. Labeled are the locations of the target and dipole magnet, as well as the bdot probe at the time of the images. The colorbar is saturated for clarity.

B. Fast-Gate Imaging

To visualize the laser-driven plasma, fast-gate images were acquired. Example images from a run at M_{950} are shown in Fig. 3. Each image is gated over 10 ns and obtained from a different laser shot. The plastic target

is located at the bottom edge of the images, and the dipole magnet center is located at the top. The bdot probe is also visible near the center of the image. The laser-ablated plasma is initially approximately spherical in shape, which is then distorted by Rayleigh-Taylor modes in the large-Larmor-radius limit⁴⁰⁻⁴². By ~ 1 μ s, the plasma has reached the dipole magnet surface. A cavity is clearly visible in the emission at earlier times, which previous LAPD experiments have shown is closely aligned with a magnetic cavity³⁵. This cavity appears to collapse by $t = 1.22$ μ s, though material continues to be emitted from the target for several more μ s.

The laser-driven plasma consists of both H ions and a range of C ionizations⁴³; however, these images only capture self-emission from the bulk, lower-ionization C components of the laser-driven plasma; the H background plasma, H-component of the laser-driven plasma, and highly-ionized C-component of the laser-driven plasma are not imaged over the wavelengths to which the camera is sensitive. Since the highly-ionized C or H ions primarily drive the interaction with the dipole magnet (since they have the smallest gyroradii), those effects are not reflected in these images. Conversely, the bulk C plasma and associated instabilities appear to have little effect on the development of a magnetosphere over the timescales analyzed.

C. Magnetosphere Measurements

The laser generates a strongly-driven plasma flow, either directly through the laser-ablated plasma or by accelerating the background plasma^{44,45}. The resulting interaction is shown in Fig. 4 for four different dipole moments and for a case with the dipole but without a background plasma or field. The data consists of 2D x - y planes taken on the "dayside," i.e. between the laser target and dipole magnet, that span from $x = -2$ to $x = 3$ cm and from $y = -16$ to $y = -9$ cm at $z = 0$ (the edge of the dipole magnet extends to $y = -7$ cm). Each plane was compiled over several thousand laser shots, as described in Sec. II. The top row consists of streak plots of the relative change in magnetic field $\Delta B_z/B_{init}$ at $x = 0.75$ cm (the location of peak dipole field), and the bottom row consists of the corresponding 2D contour plots in the x - y plane of current density $J \propto \nabla \times \Delta B_z$ at the time of peak current. The magnetic field plots were created by averaging over $x = 0.25$ to $x = 1.25$ cm and then applying a moving average along y with a width of 0.75 cm. After calculating J_x , the current density plots were similarly smoothed. A summary of the experimental runs is provided in Table I.

Figure 4(a1) shows the case with zero dipole moment $M = 0$ (the dipole magnet was inserted into the vacuum chamber but not pulsed). The laser plasma creates a diamagnetic cavity in the background plasma⁴⁶ that completely evacuates the background field ($\Delta B_z/B_{init} \approx -1$). The peak magnetic compression ($\Delta B_z/B_{init} \approx 0.3$)

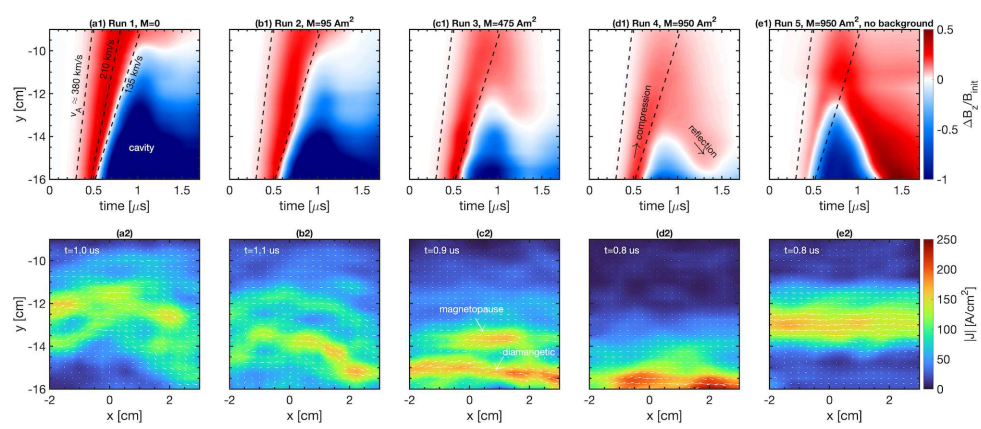


FIG. 4: (Top panels) Dayside magnetic field streak plots along y at $\{x, z\} = \{0.75, 0\}$ cm for different dipole magnetic moments M . In case (e), there is additionally no background plasma or magnetic field B_0 . The edge of the dipole magnet is located at $y = -7$ cm. The colorbars are saturated to make features more clear. (Bottom panels) 2D contour plots of the derived dayside current density in the x - y plane, taken at the time of peak current for each M . Overplotted is the current density vector field (white arrows).

363 moves at ~ 210 km/s, which we take as the speed of the
 364 laser-driven plasma. The leading edge of the compression
 365 moves at ~ 380 km/s, comparable to the Alfvén speed,
 366 while the cavity itself propagates out at approximately
 367 135 km/s. The speeds are labeled in Fig. 4(a1), and the
 368 leading and cavity speeds are shown as dashed lines for
 369 reference in Fig. 4(b1)-(e1). The cavity is supported by
 370 a strong diamagnetic current that extends across x as
 371 seen in Fig. 4(a2). After about 1.5 μ s the cavity begins
 372 to collapse as the expelled field diffuses back in. Similar
 373 behavior is observed for a low dipole moment M_{95} (see
 374 Figs. 4(b1)-(b2)).

375 Figure 4(c1) shows the case with a significantly larger
 376 dipole moment M_{475} . The laser-driven cavity and com-
 377 pression are still visible; the initial evolution of the laser-
 378 driven plasma is largely unaffected by the additional
 379 dipole field due to the $1/y^3$ falloff. However, closer to the
 380 dipole magnet, the extra magnetic pressure is able to bal-
 381 ance the plasma ram pressure, and the edge of the cavity
 382 ($\Delta B_z/B_{init} = 0$) only propagates to $y \approx -13$ cm. The
 383 magnetic compression, in turn, penetrates to the edge
 384 of the measurement region ($y = -9$ cm), but is then
 385 reflected back to $y \approx -13$ cm by the additional dipole
 386 magnetic pressure. The overall magnetic compression be-
 387 tween the cavity and dipole now lasts up to 1.5 μ s. This
 388 effect is more pronounced at the strongest dipole moment
 389 M_{950} (see Fig. 4(d1)), where the cavity is even smaller
 390 and the magnetic compression is reflected further back
 391 towards the target. Finally, Fig. 4(e1) shows streak plots
 392 for conditions identical to Fig. 4(d1), but with no back-
 393 ground plasma or background magnetic field B_0 . The
 394 lack of magnetic field near the target ($B_{dip} < 50$ G at
 395 $y = -27$ cm) leads to a weaker magnetic compression
 396 ahead of the cavity, and the cavity is able to propagate

397 closer to the dipole magnet. There is a clear reflection
 398 point around $y \approx -12$ cm, and the reflected compres-
 399 sion is significantly stronger and propagates further back
 400 towards the target compared to the M_{950} case.

401 The dipole magnetic pressure leads to additional struc-
 402 ture in the current density. Without the dipole field
 403 (Fig. 4(a1)) or without the background plasma and field
 404 (Fig. 4(e1)), the diamagnetic current propagates out in
 405 tandem with the unrestricted cavity. At M_{475} , though,
 406 there are two distinct regions of peaked current den-
 407 sity (see arrows in Fig. 4(c2)), which are also seen at
 408 M_{95} (Fig. 4(b2)), though weaker. The current structures
 409 are extended along x , consistent with the large plasma
 410 plumes created by the laser (see Fig. 3). In contrast, the
 411 M_{950} case only has one current feature at the edge of the
 412 measurement region.

413 In Figs. 4(b2)-(c2), the region with the relatively
 414 stronger current density closer to the target (farther from
 415 the dipole) is the diamagnetic current. As the cavity ex-
 416 pansion is halted, this current reaches a maximum extent
 417 and then persists for a few hundred ns before the cavity
 418 begins collapsing. The magnitude of the diamagnetic cur-
 419 rent density also increases with dipole moment. Ahead
 420 of the diamagnetic current, there is a shorter-lived region
 421 of weaker current density at M_{95} and M_{475} . As discussed
 422 in Sec. IV, this current is associated with a location of
 423 the magnetopause, i.e. the region of pressure balance be-
 424 tween the plasma ram pressure and magnetic pressure.
 425 In the M_{950} case (Fig. 4(d2)), the current density is even
 426 stronger and likely associated with the magnetopause,
 427 though it may also overlap with the diamagnetic current.
 428 In all cases, the current structures are of order d_i from
 429 the dipole and span electron scales ($\sim d_e$), emphasizing
 430 the kinetic nature of this system.

This is the author's peer reviewed, accepted manuscript. However, the online version of record will be different from this version once it has been copyedited and typeset.

PLEASE CITE THIS ARTICLE AS DOI: 10.1063/5.0084353

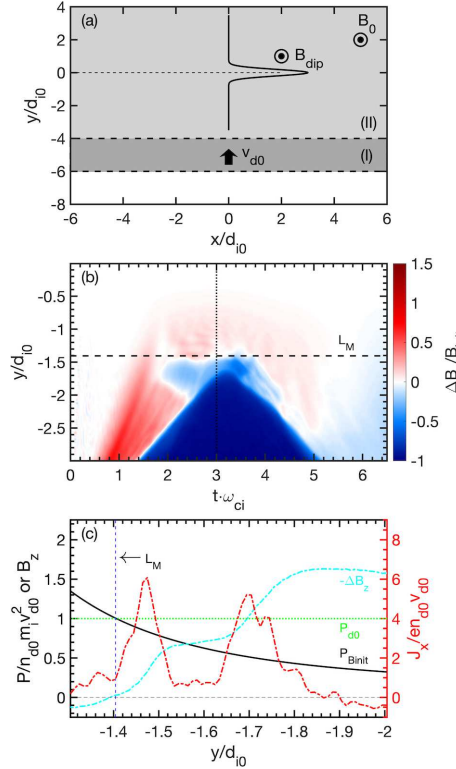


FIG. 5: Results from the 2D PIC simulation discussed in the text. (a) Simulation setup. A uniform driver plasma starts in region (I) with initial velocity v_{d0} , and the uniform magnetized background plasma starts in region (II). The dipole field B_{dip} is centered at $\{x, y\} = \{0, 0\}$. (b) Streaked contour plot of magnetic field at $x = 0$. (c) Profiles of initial magnetic pressure P_{Binit} and initial driver kinetic ram pressure P_{d0} , along with the change in magnetic field $-\Delta B_z$ and current density J_x at time $t = 3 \omega_{ci}^{-1}$ (dotted line in (b)). The pressures are defined in the text.

D. Comparison to PIC Simulations

To further interpret the experimental data, we performed 2D simulations using OSIRIS, a massively parallel, fully relativistic particle-in-cell (PIC) code^{47,48}. Using PIC allows us to accurately resolve the kinetic scales associated with mini-magnetospheres. In the simulations, a uniform slab representing the laser-driven plasma expands into a uniform background plasma embedded in a combination of a constant magnetic field B_0 and a dipole magnetic field. The simulation setup is shown in Fig. 5(a). The plasma and field parameters are chosen to be similar to those in the experiment; specifically, the dipole magnetic moment and laser-driven plasma ex-

pansion were designed so that the magnetopause stands off was $L_M = 1.4 d_{i0}$. Additionally, to reduce computational resources, a reduced electron-ion mass ratio of $m_e/m_i = 100$, increased v_{d0}/c ratio (where v_{d0} is the initial slab plasma speed), and initially cold plasmas were used. Here, we focus on key results from the simulations for comparison to the data. Additional information about the simulation setup, and detailed simulation results, are presented in Part II.

Figure 5(b) shows a streaked contour plot of the relative magnetic field $\Delta B_z/B_{init}$ along y at $x = 0$ from the simulation. As in the experiments, the expanding plasma slab drives a diamagnetic cavity and leading magnetic compression. Similarly, the compression advances past L_M and is then reflected back at later times, while the magnetic cavity is stopped near L_M . Fig. 5(c) shows lineouts from the simulation of ΔB_z at $t = 3 \omega_{ci}^{-1}$ from Fig. 5(b), as well as the current density J_x . Also plotted are the initial total magnetic pressure $P_{Binit} = B_{init}^2/2\mu_0$ and initial driver kinetic ram pressure $P_{d0} = n_{d0} m_{d0} v_{d0}^2$. As can be seen, there are two peaks in the current density corresponding to the magnetopause current (around $y \approx -1.5 d_{i0}$) and the diamagnetic current (around $y \approx -1.7 d_{i0}$).

The location of these currents is dictated by pressure and energy balances. By design, the initial driver kinetic pressure is set up to balance the total magnetic pressure, $P_{d0} = P_{Binit}$, at $L_M = 1.4 d_{i0}$. This pressure balance defines the magnetopause and is directly seen in Fig. 5(c), where the magnetopause current peaks slightly behind where $P_{d0} = P_{Binit}$. Since the laser-driven plasma acts to sweep up and accelerate the background plasma, the furthest extent of the diamagnetic current is dictated by how much of the initial driver energy is used to accelerate background plasma versus expel magnetic field. In the simulation, approximately 53% of the initial driver energy goes into the fields by time $t = 3 \omega_{ci}^{-1}$. This energy is used to expel the magnetic field from where the driver starts to the location L_{dia} of the diamagnetic current and can be written $W_B/W_{d0} = \int_{-4d_i}^{L_{dia}} P_{Binit} dy/W_{d0}$, where $W_{d0} = P_{d0} L_d$ is the initial driver energy and L_d is the width of the driver. For $W_B/W_{d0} = 0.53$, this yields $L_{dia} \approx -1.62 d_i$, consistent with the front edge of the diamagnetic current seen in Fig. 5(c).

Based on the detailed simulations presented in Part II, we make here three additional observations that are relevant to the experiments. First, both the driver and driver-accelerated background ions support the magnetopause. In the simulations, the background ions, which stream ahead of the bulk of the driver ions, initially establish a magnetopause as a pressure balance between the background ion kinetic ram pressure and the relative magnetic pressure, $P_{bg} = P_{Brel} \equiv (B_{tot}^2 - B_0^2)/2\mu_0$. The relative magnetic pressure is relevant because the background plasma is initially entrained in the background magnetic field, and so the pressure contribution from B_0 can be ignored. Later, another magnetopause is supported by both the driver and background ions where

502 $P_{d0} = P_{Binit}$, since by this time much of the background
 503 plasma has been pushed out. Meanwhile, the diamagnetic
 504 current is driven primarily by the driver plasma.

505 Second, given sufficient energy, the driver plasma will
 506 expel magnetic field up to the magnetopause, beyond
 507 which the driver plasma does not have sufficient pressure
 508 to expand further; in other words, the farthest that the
 509 diamagnetic current can be driven is L_M . In the simulations,
 510 the driver energy is primarily set by the width of
 511 the slab plasma (the initial slab velocity is held constant),
 512 with wider slabs equivalent to higher driver energies. In-
 513 creasing the slab width will thus push the diamagnetic
 514 current closer to the magnetopause location until they
 515 merge as a single current structure, which is observed in
 516 the simulations presented in Part II. In the simulation
 517 presented here, the driver slab doesn't have enough en-
 518 ergy (i.e. energy-constrained) to expel fields up to the
 519 magnetopause, resulting in the double current structure
 520 observed in Fig. 5(c). Furthermore, the reflection of the
 521 compressed field is also due to the finite driver width; the
 522 more energetic the driver, the longer the magnetopause
 523 can be maintained before the field is reflected (there is
 524 no reflection for an infinite driver).

525 Lastly, for a given driver energy, simulations observe
 526 that the separation between the magnetopause and dia-
 527 magnetic current decreases with increasing dipole mo-
 528 ment M . This can be understood as follows. On the
 529 one hand increasing M will push the magnetopause lo-
 530 cation L_M farther from the dipole and closer to the lo-
 531 cation of the diamagnetic current L_{dia} . On the other
 532 hand, the increase in magnetic field amplitude means
 533 that the the driver depletes a larger fraction of its en-
 534 ergy per unit length over the propagated distance, result-
 535 ing in a smaller diamagnetic cavity. For a fixed amount
 536 of energy into the fields, L_{dia} will increase faster than
 537 L_M as M increases, seemingly implying that the sepa-
 538 ration between the magnetopause and diamagnetic cur-
 539 rent should increase with dipole moment. However, the
 540 driver also sweeps out a smaller region of background
 541 plasma, resulting in less relative energy going into the
 542 background plasma and more energy available to expel
 543 the fields. This extra energy is sufficient to compensate
 544 for the larger fields and allows the driver to push the
 545 diamagnetic current closer to the magnetopause.

546 IV. DISCUSSION

547 Based on the signatures observed in the simulations, in
 548 Fig. 6 we plot lineouts of the current density at $x = 0.75$
 549 cm for three cases of M taken from Figs. 4(a2), (c2),
 550 and (e2). Also plotted are the total initial magnetic
 551 pressure P_{Binit} and change in magnetic field $-\Delta B_z$.
 552 With a background plasma and background field, but
 553 no dipole field ($M = 0$, see Fig. 6(a)), the driver pressure
 554 is greater than the initial magnetic pressure everywhere
 555 ($P_{d0} > P_{Binit}$), and there is no pressure balance, and
 556 hence no magnetopause. Thus, the only current struc-

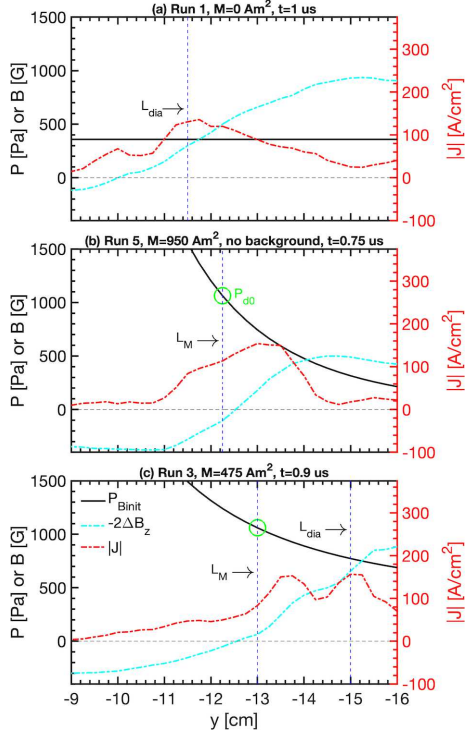


FIG. 6: Dayside current density J (red) at $x = 0.75$ cm for three M from Figs. 4(a2), (c2), and (e2). Also plotted are the total initial magnetic pressure P_{Binit} (solid black), change in magnetic field $-\Delta B_z$ (cyan), and the approximate location of the magnetopause L_M or diamagnetic L_{dia} currents (blue). The green circle indicates the initial driver pressure P_{d0} needed to balance the initial magnetic pressure P_{Binit} at the location of the magnetopause.

557 ture created is the diamagnetic current as the driver
 558 plasma expands out. The approximate final position
 559 L_{dia} of the diamagnetic current is shown in Fig. 6(a).
 560 We can estimate the total initial driver energy per area
 561 \bar{W}_{d0} as the sum of the energy needed to expel the field
 562 $\bar{W}_B = \int_{L_{tar}}^{L_{dia}} B_0^2 / 2\mu_0 dy$ and sweep out the background
 563 plasma $\bar{W}_{bg} = \int_{L_{tar}}^{L_{dia}} n_0 m_i v_0^2 dy$ between the target po-
 564 sition L_{tar} and L_{dia} , assuming a uniform background
 565 plasma. For the parameters in Table I and $L_{tar} = -27.5$
 566 cm, we find $\bar{W}_{d0} \approx 90$ J/m².
 567 Figure 6(b) shows the case where there is no back-
 568 ground plasma or magnetic field, and the driver plasma
 569 expands into just the dipole magnetic field. Here, the
 570 driver will expand out, creating a diamagnetic cavity,
 571 until it reaches a pressure balance with the total initial
 572 magnetic field ($P_{d0} = P_{Binit}$) or runs out of energy. The

573 energy required to expel the field in Fig. 6(b) is only
 574 $\bar{W}_{d0} \approx 30 \text{ J/m}^2$. Since the driver plasma is effectively
 575 identical between all runs, this indicates that the driver
 576 plasma is not energy-constrained and instead reaches the
 577 magnetopause. Based on the location of the magne-
 578 topause L_M in Fig. 6(b) (taken where $\Delta B_z \approx 0$) and
 579 the pressure balance $P_{d0} = P_{Binit}$, we can then estimate
 580 $P_{d0} \approx 1050 \text{ Pa}$. This is reasonable since it only requires
 581 an average drive plasma density $n_{d0} \approx 10^{13} \text{ cm}^{-3}$ and
 582 speed $v_{d0} \approx 250 \text{ km/s}$, easily attainable in the exper-
 583 iments.

584 We expect the same initial driver pressure in Fig. 6(c),
 585 and the location of $P_{d0} = P_{Binit}$ is shown as the green
 586 circle. As in the simulations, the location of this pressure
 587 balance is coincident with the location where $\Delta B_z \approx 0$,
 588 and slightly behind it ($y \approx -13.5 \text{ cm}$) we observe a peak
 589 in the current density consistent with the magnetopause
 590 current. Also like the simulations, further from the mag-
 591 netopause ($y \approx -15 \text{ cm}$) we find the diamagnetic cur-
 592 rent. Following a similar calculation as above and us-
 593 ing the location of L_{dia} shown in Fig. 6(c), we can esti-
 594 mate the energy needed to expel the fields and sweep out
 595 background plasma. The total driver energy needed is
 596 $\bar{W}_{d0} \approx 90 \text{ J/m}^2$, which is the same as in Fig. 6(a). This
 597 implies that the driver plasma does not have enough en-
 598 ergy to drive the diamagnetic current all the way to the
 599 magnetopause, also consistent with the simulations.

600 At $M = 95 \text{ Am}^2$, the driver plasma would not reach
 601 pressure balance until very close to the dipole, beyond the
 602 measurement region. Since the observed current struc-
 603 tures only reach $y \approx -12 \text{ cm}$ (see Fig. 4(b2)), this indi-
 604 cates that here too the driver plasma runs out of energy
 605 before reaching the magnetopause, similar to Fig. 6(c).
 606 Taking the current structure at $y \approx -13.75 \text{ cm}$ as the
 607 diamagnetic current, the total driver energy needed is
 608 $\bar{W}_{d0} \approx 80 \text{ J/m}^2$. Given the much weaker dipole field,
 609 the weak current structure ahead of the diamagnetic cur-
 610 rent may be a magnetopause driven by background ions
 611 rather than driver ions as in the other cases. A typical
 612 background kinetic pressure would be $P_{bg} \sim 100-200 \text{ Pa}$
 613 for the values in Table I, too low to account for the fea-
 614 tures in the larger M cases but sufficient to balance P_{Brel}
 615 near $y \approx -11 \text{ cm}$.

616 Finally, it is difficult to conclude anything from the
 617 highest moment case $M = 950 \text{ Am}^2$ (see Fig. 4(d2)).
 618 Assuming the same initial driver pressure, the magne-
 619 topause would be located at $y \approx -16 \text{ cm}$, right at the
 620 edge of the measurement region. Assuming the same
 621 initial driver energy, we would expect the diamagnetic
 622 current to be located around $y \approx -17 \text{ cm}$ (outside the
 623 measurement region). The observed current structure
 624 could thus be the magnetopause current. The diamag-
 625 netic current would also be closer to the magnetopause
 626 than at lower M , consistent with the simulations.

627 V. CONCLUSIONS

628 In this paper, we have presented preliminary results
 629 from a new experimental platform to study strongly-
 630 driven ion-scale magnetospheres. The platform – in-
 631 cluding background magnetized plasma, target and laser-
 632 driven plasma, pulsed dipole magnet, and diagnostics –
 633 can be run at high repetition rate ($\sim 1 \text{ Hz}$), allowing
 634 detailed 2D measurements of the magnetic field evolu-
 635 tion acquired over thousands of shots. Data with four
 636 different dipole moments ($M = 0, 95, 475$, and 950 Am^2)
 637 was collected. In the absence of a dipole field, only the
 638 magnetic cavity and associated diamagnetic current from
 639 the laser-driven plasma were observed. In contrast, for
 640 $M > 0$ a magnetopause current, in addition to the dia-
 641 magnetic current, was observed on kinetic ion and elec-
 642 tron scales (i.e. of order d_i and d_e), indicating the for-
 643 mation of a mini-magnetosphere.

644 The experimental results were compared to 2D PIC
 645 simulations using the code OSIRIS. The simulations re-
 646 produce the basic magnetic field structures seen in the ex-
 647 periments, including the magnetic compression and cav-
 648 ity formed by the laser-driven plasma, and the reflection
 649 of the compression by the dipole pressure. The simula-
 650 tions confirm that the location of the magnetopause is
 651 dictated by the balance between the initial driver kinetic
 652 ram pressure and the initial total magnetic field pres-
 653 sure. However, dynamically the magnetopause current
 654 is supported by both the background and laser-driven
 655 ions (though the current itself is carried by the elec-
 656 trons) and a complicated time-dependent combination of
 657 driver pressure balance and the pressure balance between
 658 background ion ram pressure and the relative magnetic
 659 pressure (i.e. total magnetic pressure minus the pressure
 660 from the constant background field). The signatures of
 661 these pressure balances, derived from the simulations, are
 662 also observed in the experiments. Lastly, the simulations
 663 show that as the dipole moment is increased, the location
 664 of the magnetopause is pushed further from the dipole.
 665 This results in a shrinking separation between the mag-
 666 netopause and diamagnetic currents, and even overlap-
 667 ping current structures, features that are observed in the
 668 experiments.

669 While the experiments employed a double cathode
 670 setup to create a high density background plasma in the
 671 core of the LAPD, the constrained size of the high-density
 672 core meant that the laser-driven plasma mostly expanded
 673 through a lower density background plasma. This re-
 674 sulted in a primarily sub-Alfvénic ($M_A \approx 0.6$) interaction
 675 and a Hall parameter of $D \approx 1$. The LAPD has recently
 676 implemented a new large-diameter LaB_6 cathode that
 677 will make most of the background plasma higher density,
 678 enabling both super-Alfvénic expansions ($D > M_A > 1$)
 679 and the study of bow shocks.

680 Future experiments will focus on three main objectives.
 681 First, we will take advantage of the high-repetition-rate
 682 platform to expand the 2D planes measured here into
 683 3D cubes to obtain fully 3D magnetic field and current

This is the author's peer reviewed, accepted manuscript. However, the online version of record will be different from this version once it has been copyedited and typeset.

PLEASE CITE THIS ARTICLE AS DOI: 10.1063/5.0084353

684 density profiles. Second, in addition to the "dayside" we 744 will measure other regions around the dipole, including 745 the "nightside" opposite the laser target. Finally, we will 746 deploy a magnetic field configuration in which the dipole 747 and background fields are anti-aligned in the measure- 748 ment region (they were aligned in the experiments pre- 749 sented here). This will allow magnetic reconnection in 750 the "subsol" region to be studied and contrasted with 751 the configuration explored in this paper, in which any 752 reconnection would have been dominantly poleward.

694 **ACKNOWLEDGMENTS**

695 We are grateful to the staff of the BaPSF for their help 753 in carrying out these experiments. The experiments were 754 supported by the DOE under Grants No. DE-SC0008655 755 and No. DE-SC00016249, by the NSF/DOE Partner- 756 ship in Basic Plasmas Science and Engineering Award 757 No. PHY-2010248, and by the Defense Threat Reduction 758 Agency and Lawrence Livermore National Security LLC 759 under contract No. B643014. The simulations were sup- 760 ported by the European Research Council (InPairs ERC- 761 2015-AdG 695088) and FCT (PD/BD/114307/2016 and 762 APPLAuSE PD/00505/2012). Access to MareNostrum 763 (Barcelona Supercomputing Center, Spain) was awarded 764 through PRACE, and simulations were performed at the 765 IST cluster (Lisbon, Portugal) and at MareNostrum.

709 ¹T. Pulkkinen, "Space weather: terrestrial perspective," *Living 710 Reviews in Solar Physics* **4**, 1 (2007).

711 ²J. P. Eastwood, "The science of space weather," *Philosophical 712 Transactions of the Royal Society A: Mathematical, Physical and 713 Engineering Sciences* **366**, 4489–4500 (2008).

714 ³C. T. Russell, *Space Physics: An Introduction* (Cambridge Uni- 715 versity Press, 2016).

716 ⁴J. E. Borovsky and J. A. Valdovinos, *Surveys in Geophysics*, Vol. 39 717 (Springer Netherlands, 2018) pp. 817–859.

718 ⁵N. Omidi, X. Blanco-Cano, C. Russell, and H. Karimabadi, 719 "Dipolar magnetospheres and their characterization as a function 720 of magnetic moment," *Adv. in Space Res.* **33**, 1996 (2004).

721 ⁶I. Shaikhislamov, V. Antonov, Y. Zakharov, E. Boyarintsev, 722 A. Melekhov, V. Posukh, and A. Ponomarenko, "Minim- 723 magnetosphere: Laboratory experiment, physical model and hall 724 MHD simulation," *Adv. in Space Res.* **52**, 422 – 436 (2013).

725 ⁷H. Nilsson, G. Stenberg Wieser, E. Behar, C. S. Wedlund, 726 H. Gunell, M. Yamauchi, R. Lundin, S. Barabash, M. Wieser, 727 C. Carr, E. Cupido, J. L. Burch, A. Fedorov, J.-A. Sauvage, 728 H. Koskinen, E. Kallio, J.-P. Lebreton, A. Eriksson, N. Edberg, 729 R. Goldstein, P. Henri, C. Koenders, P. Mokashi, Z. Nemeth, 730 I. Richter, K. Szego, M. Volwerk, C. Vallat, and M. Rubin, "Birth 731 of a comet magnetosphere: A spring of water ions," *Science* **347** 732 (2015).

733 ⁸J. Halekas, G. Delory, D. Brain, R. Lin, and D. Mitchell, "Density 734 cavity observed over a strong lunar crustal magnetic anomaly in 735 the solar wind: A mini-magnetosphere?" *Planetary and Space 736 Science* **56**, 941 – 946 (2008).

737 ⁹M. Wieser, S. Barabash, Y. Futaana, M. Holmström, A. Bhard- 738 waj, R. Sridharan, M. B. Dhanya, A. Schauflerberger, P. Wurz, 739 and K. Asamura, "First observation of a mini-magnetosphere 740 above a lunar magnetic anomaly using energetic neutral atoms," 741 *Geophysical Research Letters* **37** (2010).

742 ¹⁰C. Lue, Y. Futaana, S. Barabash, M. Wieser, M. Holmström, 743 A. Bhardwaj, M. B. Dhanya, and P. Wurz, "Strong influence of 744 lunar crustal fields on the solar wind flow," *Geophysical Research Letters* **38** (2011).

745 ¹¹R. A. Bamford, B. Kellett, W. J. Bradford, C. Norberg, 746 A. Thornton, K. J. Gibson, I. A. Crawford, L. Silva, L. Gargate, 747 and R. Bingham, "Minimagnetospheres above the lunar surface 748 and the formation of lunar swirls," *Phys. Rev. Lett.* **109**, 081101 749 (2012).

750 ¹²J. S. Halekas, A. R. Poppe, J. P. McFadden, V. Angelopoulos, 751 K.-H. Glassmeier, and D. A. Brain, "Evidence for small-scale 752 collisionless shocks at the moon from artemis," *Geophysical Re- 753 search Letters* **41**, 7436–7443 (2014).

754 ¹³T. Moritaka, Y. Kajimura, H. Usui, M. Matsumoto, T. Matsui, 755 and I. Shinohara, "Momentum transfer of solar wind plasma in 756 a kinetic scale magnetosphere," *Physics of Plasmas* **19**, 032111 757 (2012).

758 ¹⁴H. Karimabadi, V. Roytershteyn, H. X. Vu, Y. A. Omelchenko, 759 J. Scudder, W. Daughton, A. Dimmock, K. Nykyri, M. Wan, 760 D. Sibeck, M. Tatíneni, A. Majumdar, B. Loring, and B. Geveci, 761 "The link between shocks, turbulence, and magnetic recon- 762 cession in collisionless plasmas," *Physics of Plasmas* **21** (2014).

763 ¹⁵W. Gonzalez and E. Parker, eds., *Magnetic Reconnection* 764 (Springer International Publishing, 2016).

765 ¹⁶D. Winske, L. Yin, N. Omidi, H. Karimabadi, and K. Quest, 766 "Hybrid simulations codes: Past, present and future - a tutorial," 767 Tech. Rep. (2003).

768 ¹⁷Y. Lin and X. Y. Wang, "Three-dimensional global hybrid sim- 769 ulation of dayside dynamics associated with the quasi-parallel 770 bow shock," *Journal of Geophysical Research: Space Physics* **110** 771 (2005).

772 ¹⁸X. Blanco-Cano, N. Omidi, and C. T. Russell, "Global hybrid 773 simulations: Foreshock waves and cavitons under radial inter- 774 planetary magnetic field geometry," *Journal of Geophysical Re- 775 search: Space Physics* **114** (2009).

776 ¹⁹Y. A. Omelchenko, V. Roytershteyn, L.-J. Chen, J. Ng, and 777 H. Hietala, "Hypers simulations of solar wind interactions with 778 the earth's magnetosphere and the moon," *Journal of Atmo- 779 pheric and Solar-Terrestrial Physics* **215**, 105581 (2021).

780 ²⁰Y. Vernisse, J. Riouset, U. Motschmann, and K.-H. Glassmeier, 781 "Stellar winds and planetary bodies simulations: Magnetized ob- 782 stacles in super-alfvénic and sub-alfvénic flows," *Planetary and 783 Space Science* **137**, 40 – 51 (2017).

784 ²¹J. Deca, P. Henri, A. Divin, A. Eriksson, S. Markidis, V. Ol- 785 sheshevsky, and M. Horányi, "Electron and ion dynamics of the 786 solar wind interaction with a weakly outgassing comet," *Phys. 787 Rev. Lett.* **118**, 205101 (2017).

788 ²²J. Deca, P. Henri, A. Divin, A. Eriksson, M. Galand, A. Beth, 789 K. Ostaszewski, and M. Horányi, "Building a weakly outgassing 790 comet from a generalized ohm's law," *Phys. Rev. Lett.* **123**, 791 055101 (2019).

792 ²³N. Omidi, X. Blanco-Cano, C. T. Russell, H. Karimabadi, and 793 M. Acuna, "Hybrid simulations of solar wind interaction with 794 magnetized asteroids: General characteristics," *J. Geophys. Res.* 795 **107**, 1487 (2002).

796 ²⁴N. Omidi, X. Blanco-Cano, and C. T. Russell, "Macrostructure 797 of collisionless bow shocks: 1. scale lengths," *J. Geophys. Res.* 798 **110** (2005).

799 ²⁵L. Gargaté, R. Bingham, R. A. Fonseca, R. Bamford, A. Thor- 800 nton, K. Gibson, J. Bradford, and L. O. Silva, "Hybrid sim- 801 ulations of mini-magnetospheres in the laboratory," *Plasma Phys. 802 and Controlled Fusion* **50**, 074017 (2008).

803 ²⁶F. Cruz, E. P. Alves, R. A. Bamford, R. Bingham, R. A. Fonseca, 804 and L. O. Silva, "Formation of collisionless shocks in magnetized 805 plasma interaction with kinetic-scale obstacles," *Phys. Plasmas* 806 **24**, 022901 (2017).

807 ²⁷G. Yur, H. U. Rahman, J. Birn, F. J. Wessel, and S. Minami, 808 "Laboratory facility for magnetospheric simulation," *Journal of 809 Geophysical Research: Space Physics* **100**, 23727–23736 (1995).

810 ²⁸G. Yur, T.-F. Chang, H. U. Rahman, J. Birn, and C. K. Chao, 811 "Magnetotail structures in a laboratory magnetosphere," *Jour- 812 nal of Geophysical Research: Space Physics* **104**, 14517–14528 813 (1999).

This is the author's peer reviewed, accepted manuscript. However, the online version of record will be different from this version once it has been copyedited and typeset.

PLEASE CITE THIS ARTICLE AS DOI: 10.1063/5.0084353

This is the author's peer reviewed, accepted manuscript. However, the online version of record will be different from this version once it has been copyedited and typeset.

814 (1999).

815 ²⁹P. Brady, T. Ditmire, W. Horton, M. L. Mays, and Y. Zakharov, 858 ³⁹P. Heuer, D. Schaeffer, E. Knall, C. Constantin, L. Hofer, S. Vincena, S. Tripathi, and C. Niemann, "Fast gated imaging of the

816 "Laboratory experiments simulating solar wind driven magnetospheres," *Phys. Plasmas* **16**, 043112 (2009). 859 collisionless interaction of a laser-produced and magnetized ambient plasma," *High Energy Density Physics* **22**, 17 (2017).

817 ³⁰Y. P. Zakharov, A. G. Ponomarenko, K. V. Vchivkov, W. Horton, 860 ⁴⁰B. H. Ripin, E. A. McLean, C. K. Manka, C. Pawley, J. A. Stamper, T. A. Peyer, A. N. Mostovych, J. Grun, A. B. Hassam, and J. Huba, "Large-larmor-radius interchange instability," *Phys. Rev. Lett.* **59**, 2299–2302 (1987).

818 and P. Brady, "Laser-plasma simulations of artificial magnetospheres formed by giant coronal mass ejections," *Astro. and 861 ⁴¹J. D. Huba, J. G. Lyon, and A. B. Hassam, "Theory and simulation of the rayleigh-taylor instability in the limit of large larmor radius," *Phys. Rev. Lett.* **59**, 2971–2974 (1987).*

819 ³¹I. F. Shaikhislamov, Y. P. Zakharov, V. G. Posukh, A. V. 862 ⁴²A. Collette and W. Gekelman, "Structure of an exploding Laser-produced plasma," *Phys. Rev. Lett.* **105**, 195003 (2010).

820 Melekhov, V. M. Antonov, E. L. Boyarinsev, and A. G. Ponomarenko, 863 ⁴³D. B. Schaeffer, A. S. Bondarenko, E. T. Everson, S. E. Clark, C. G. Constantin, and C. Niemann, "Characterization of laser-produced carbon plasmas relevant to laboratory astrophysics," *Journal of Applied Physics* **120**, 043301 (2016).

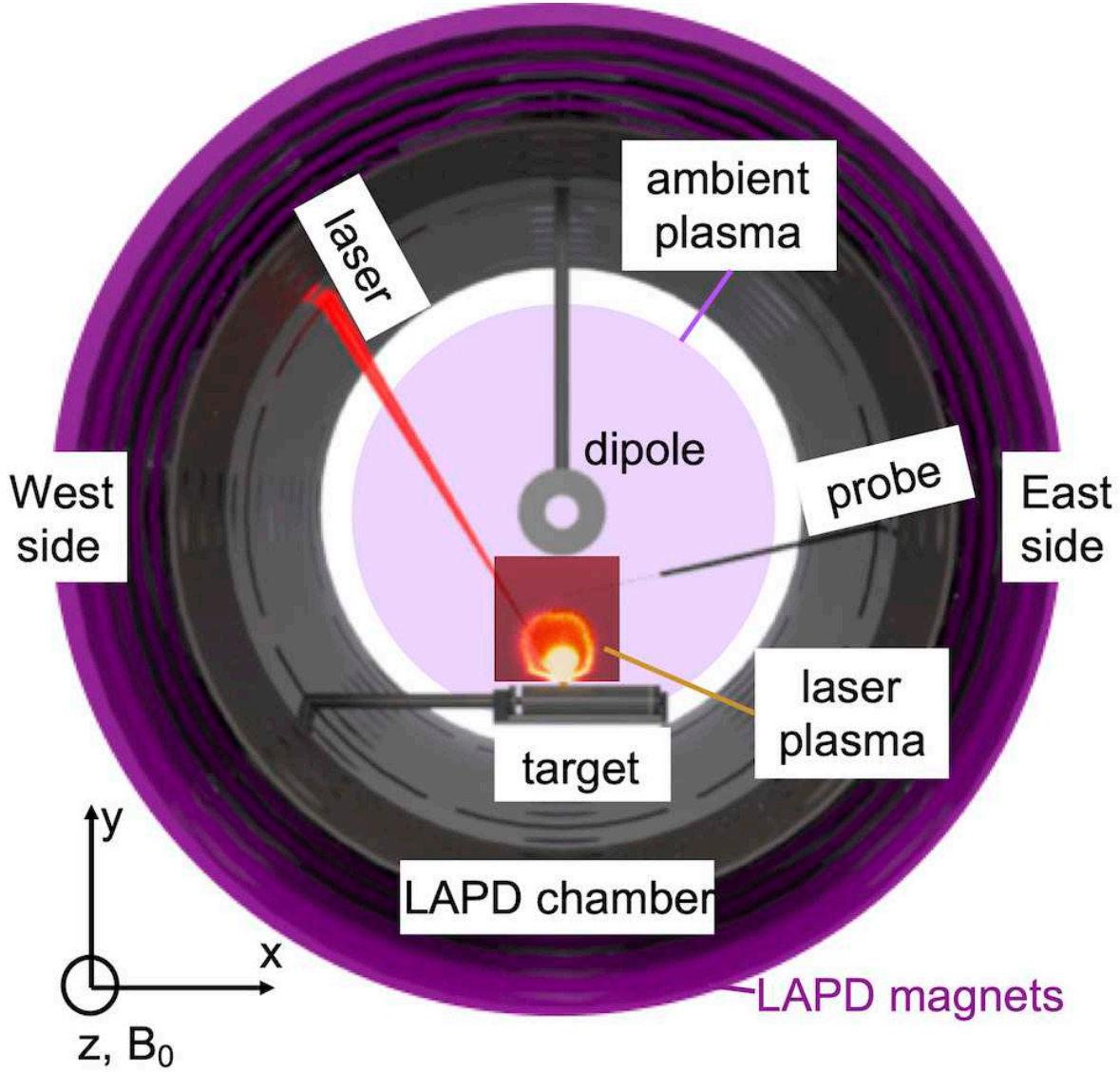
821 "Laboratory model of magnetosphere created by strong plasma perturbation with frozen-in magnetic field," *Plasma Phys. and Controlled Fusion* **56**, 125007 (2014). 864 ⁴⁴A. S. Bondarenko, D. B. Schaeffer, E. T. Everson, S. E. Clark, B. R. Lee, C. G. Constantin, S. Vincena, B. Van Compernolle, S. K. P. Tripathi, D. Winske, and C. Niemann, "Collisionless momentum transfer in space and astrophysical explosions," *Nat. Phys.* **13**, 573 (2017).

822 ³²F. Cruz, D. Schaeffer, F. Cruz, and L. Silva, "Laser-driven, ion-scale magnetospheres in laboratory plasmas. II. Particle-in-cell 865 ⁴⁵A. S. Bondarenko, D. B. Schaeffer, E. T. Everson, S. E. Clark, simulations," (2021), submitted to *Physics of Plasmas*.

823 ³³W. Gekelman, H. Pfister, Z. Lucky, J. Bamber, D. Leneman, 866 ⁴⁶C. Niemann, W. Gekelman, C. G. Constantin, E. T. Everson, D. B. Schaeffer, S. E. Clark, D. Winske, A. B. Zylstra, P. Pribyl, and J. Maggs, "Design, construction, and properties of the large 867 ⁴⁷R. A. Fonseca, L. O. Silva, F. S. Tsung, V. K. Decyk, W. Lu, plasma research device-The LAPD at UCLA," *Review of Scientific Instruments* **62**, 2875 (1991).

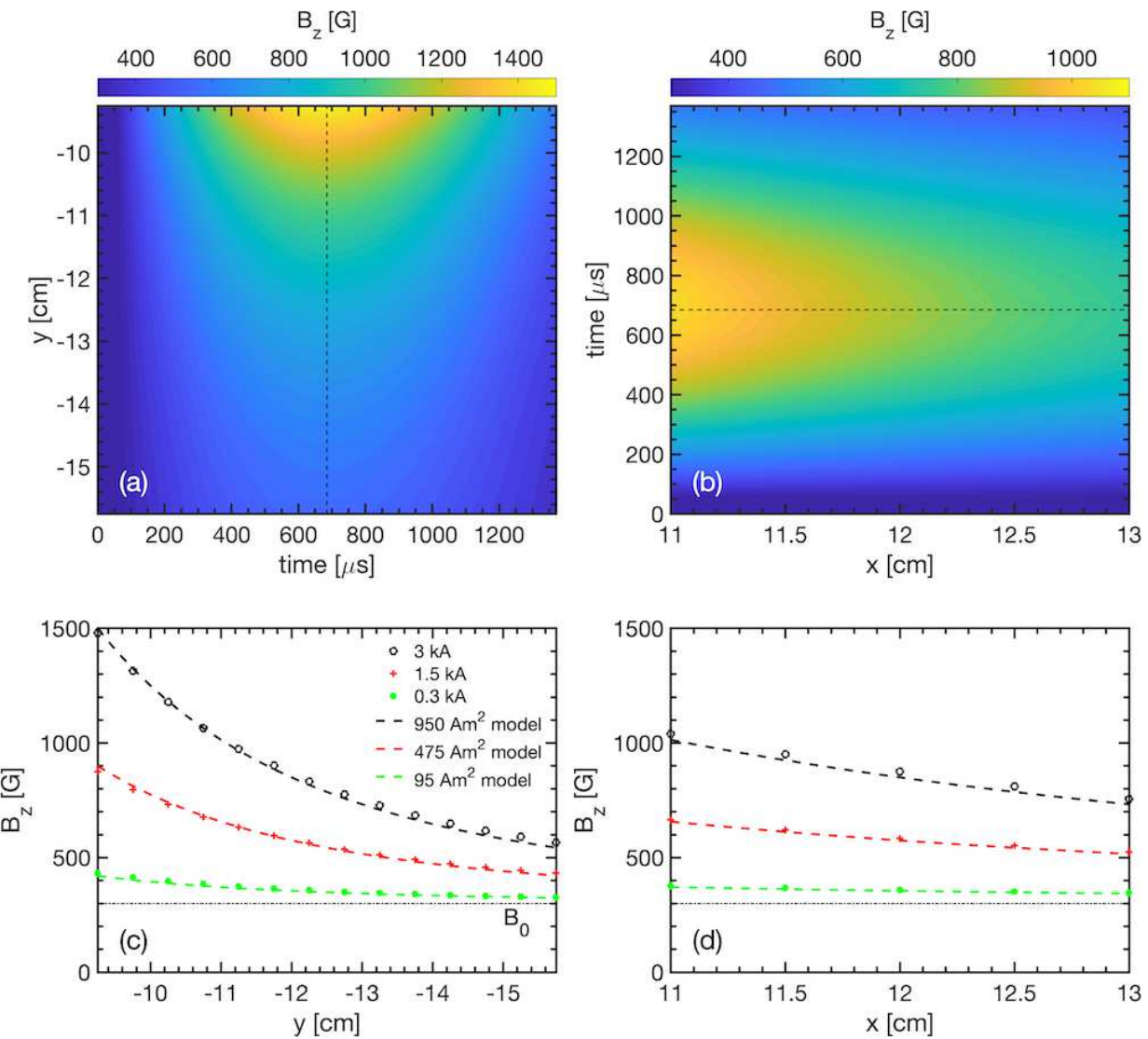
824 ³⁴C. Dane, L. Zapata, W. Neuman, M. Norton, and L. Hackel, 868 ⁴⁸R. A. Fonseca, J. Vieira, F. Fiua, A. Davidson, F. S. Tsung, "Design and operation of a 150 w near diffraction-limited laser 869 ⁴⁹W. Gekelman, H. Pfister, Z. Lucky, M. Drandell, D. Leneman, 870 ⁵⁰W. Gekelman, P. Pribyl, E. Everson, D. Schaeffer, N. L. Kugland, R. Presura, S. Neff, C. Plechaty, S. Vincena, A. Collette, S. Tripathi, M. Muniz, and C. Niemann, "Collisionless interaction of an energetic laser produced plasma with a large 871 ⁵¹E. T. Everson, P. Pribyl, C. G. Constantin, A. Zylstra, D. Schaeffer, N. L. Kugland, and C. Niemann, "Design, construction, 872 ⁵²Y. P. Zakharov, A. G. Ponomarenko, K. V. Vchivkov, W. Horton, and calibration of a three-axis, high-frequency magnetic probe (B-dot probe) as a diagnostic for exploding plasmas," *Review of 873 ⁵³W. Gekelman, P. Pribyl, Z. Lucky, M. Drandell, D. Leneman, 874 ⁵⁴Y. P. Zakharov, A. G. Ponomarenko, K. V. Vchivkov, W. Horton, 875 ⁵⁵W. Gekelman, P. Pribyl, Z. Lucky, M. Drandell, D. Leneman, 876 ⁵⁶Y. P. Zakharov, A. G. Ponomarenko, K. V. Vchivkov, W. Horton, 877 ⁵⁷Y. P. Zakharov, A. G. Ponomarenko, K. V. Vchivkov, W. Horton, 878 ⁵⁸Y. P. Zakharov, A. G. Ponomarenko, K. V. Vchivkov, W. Horton, 879 ⁵⁹Y. P. Zakharov, A. G. Ponomarenko, K. V. Vchivkov, W. Horton, 880 ⁶⁰Y. P. Zakharov, A. G. Ponomarenko, K. V. Vchivkov, W. Horton, 881 ⁶¹Y. P. Zakharov, A. G. Ponomarenko, K. V. Vchivkov, W. Horton, 882 ⁶²Y. P. Zakharov, A. G. Ponomarenko, K. V. Vchivkov, W. Horton, 883 ⁶³Y. P. Zakharov, A. G. Ponomarenko, K. V. Vchivkov, W. Horton, 884 ⁶⁴Y. P. Zakharov, A. G. Ponomarenko, K. V. Vchivkov, W. Horton, 885 ⁶⁵Y. P. Zakharov, A. G. Ponomarenko, K. V. Vchivkov, W. Horton, 886 ⁶⁶Y. P. Zakharov, A. G. Ponomarenko, K. V. Vchivkov, W. Horton, 887 ⁶⁷Y. P. Zakharov, A. G. Ponomarenko, K. V. Vchivkov, W. Horton, 888 ⁶⁸Y. P. Zakharov, A. G. Ponomarenko, K. V. Vchivkov, W. Horton, 889 ⁶⁹Y. P. Zakharov, A. G. Ponomarenko, K. V. Vchivkov, W. Horton, 890 ⁷⁰Y. P. Zakharov, A. G. Ponomarenko, K. V. Vchivkov, W. Horton, 891 ⁷¹Y. P. Zakharov, A. G. Ponomarenko, K. V. Vchivkov, W. Horton, 892 ⁷²Y. P. Zakharov, A. G. Ponomarenko, K. V. Vchivkov, W. Horton, 893 ⁷³Y. P. Zakharov, A. G. Ponomarenko, K. V. Vchivkov, W. Horton, 894 ⁷⁴Y. P. Zakharov, A. G. Ponomarenko, K. V. Vchivkov, W. Horton, 895 ⁷⁵Y. P. Zakharov, A. G. Ponomarenko, K. V. Vchivkov, W. Horton, 896 ⁷⁶Y. P. Zakharov, A. G. Ponomarenko, K. V. Vchivkov, W. Horton, 897 ⁷⁷Y. P. Zakharov, A. G. Ponomarenko, K. V. Vchivkov, W. Horton, 898 ⁷⁸Y. P. Zakharov, A. G. Ponomarenko, K. V. Vchivkov, W. Horton, 899 ⁷⁹Y. P. Zakharov, A. G. Ponomarenko, K. V. Vchivkov, W. Horton, 900 ⁸⁰Y. P. Zakharov, A. G. Ponomarenko, K. V. Vchivkov, W. Horton, 901 ⁸¹Y. P. Zakharov, A. G. Ponomarenko, K. V. Vchivkov, W. Horton, 902 ⁸²Y. P. Zakharov, A. G. Ponomarenko, K. V. Vchivkov, W. Horton, 903 ⁸³Y. P. Zakharov, A. G. Ponomarenko, K. V. Vchivkov, W. Horton, 904 ⁸⁴Y. P. Zakharov, A. G. Ponomarenko, K. V. Vchivkov, W. Horton, 905 ⁸⁵Y. P. Zakharov, A. G. Ponomarenko, K. V. Vchivkov, W. Horton, 906 ⁸⁶Y. P. Zakharov, A. G. Ponomarenko, K. V. Vchivkov, W. Horton, 907 ⁸⁷Y. P. Zakharov, A. G. Ponomarenko, K. V. Vchivkov, W. Horton, 908 ⁸⁸Y. P. Zakharov, A. G. Ponomarenko, K. V. Vchivkov, W. Horton, 909 ⁸⁹Y. P. Zakharov, A. G. Ponomarenko, K. V. Vchivkov, W. Horton, 910 ⁹⁰Y. P. Zakharov, A. G. Ponomarenko, K. V. Vchivkov, W. Horton, 911 ⁹¹Y. P. Zakharov, A. G. Ponomarenko, K. V. Vchivkov, W. Horton, 912 ⁹²Y. P. Zakharov, A. G. Ponomarenko, K. V. Vchivkov, W. Horton, 913 ⁹³Y. P. Zakharov, A. G. Ponomarenko, K. V. Vchivkov, W. Horton, 914 ⁹⁴Y. P. Zakharov, A. G. Ponomarenko, K. V. Vchivkov, W. Horton, 915 ⁹⁵Y. P. Zakharov, A. G. Ponomarenko, K. V. Vchivkov, W. Horton, 916 ⁹⁶Y. P. Zakharov, A. G. Ponomarenko, K. V. Vchivkov, W. Horton, 917 ⁹⁷Y. P. Zakharov, A. G. Ponomarenko, K. V. Vchivkov, W. Horton, 918 ⁹⁸Y. P. Zakharov, A. G. Ponomarenko, K. V. Vchivkov, W. Horton, 919 ⁹⁹Y. P. Zakharov, A. G. Ponomarenko, K. V. Vchivkov, W. Horton, 920 ¹⁰⁰Y. P. Zakharov, A. G. Ponomarenko, K. V. Vchivkov, W. Horton, 921 ¹⁰¹Y. P. Zakharov, A. G. Ponomarenko, K. V. Vchivkov, W. Horton, 922 ¹⁰²Y. P. Zakharov, A. G. Ponomarenko, K. V. Vchivkov, W. Horton, 923 ¹⁰³Y. P. Zakharov, A. G. Ponomarenko, K. V. Vchivkov, W. Horton, 924 ¹⁰⁴Y. P. Zakharov, A. G. Ponomarenko, K. V. Vchivkov, W. Horton, 925 ¹⁰⁵Y. P. Zakharov, A. G. Ponomarenko, K. V. Vchivkov, W. Horton, 926 ¹⁰⁶Y. P. Zakharov, A. G. Ponomarenko, K. V. Vchivkov, W. Horton, 927 ¹⁰⁷Y. P. Zakharov, A. G. Ponomarenko, K. V. Vchivkov, W. Horton, 928 ¹⁰⁸Y. P. Zakharov, A. G. Ponomarenko, K. V. Vchivkov, W. Horton, 929 ¹⁰⁹Y. P. Zakharov, A. G. Ponomarenko, K. V. Vchivkov, W. Horton, 930 ¹¹⁰Y. P. Zakharov, A. G. Ponomarenko, K. V. Vchivkov, W. Horton, 931 ¹¹¹Y. P. Zakharov, A. G. Ponomarenko, K. V. Vchivkov, W. Horton, 932 ¹¹²Y. P. Zakharov, A. G. Ponomarenko, K. V. Vchivkov, W. Horton, 933 ¹¹³Y. P. Zakharov, A. G. Ponomarenko, K. V. Vchivkov, W. Horton, 934 ¹¹⁴Y. P. Zakharov, A. G. Ponomarenko, K. V. Vchivkov, W. Horton, 935 ¹¹⁵Y. P. Zakharov, A. G. Ponomarenko, K. V. Vchivkov, W. Horton, 936 ¹¹⁶Y. P. Zakharov, A. G. Ponomarenko, K. V. Vchivkov, W. Horton, 937 ¹¹⁷Y. P. Zakharov, A. G. Ponomarenko, K. V. Vchivkov, W. Horton, 938 ¹¹⁸Y. P. Zakharov, A. G. Ponomarenko, K. V. Vchivkov, W. Horton, 939 ¹¹⁹Y. P. Zakharov, A. G. Ponomarenko, K. V. Vchivkov, W. Horton, 940 ¹²⁰Y. P. Zakharov, A. G. Ponomarenko, K. V. Vchivkov, W. Horton, 941 ¹²¹Y. P. Zakharov, A. G. Ponomarenko, K. V. Vchivkov, W. Horton, 942 ¹²²Y. P. Zakharov, A. G. Ponomarenko, K. V. Vchivkov, W. Horton, 943 ¹²³Y. P. Zakharov, A. G. Ponomarenko, K. V. Vchivkov, W. Horton, 944 ¹²⁴Y. P. Zakharov, A. G. Ponomarenko, K. V. Vchivkov, W. Horton, 945 ¹²⁵Y. P. Zakharov, A. G. Ponomarenko, K. V. Vchivkov, W. Horton, 946 ¹²⁶Y. P. Zakharov, A. G. Ponomarenko, K. V. Vchivkov, W. Horton, 947 ¹²⁷Y. P. Zakharov, A. G. Ponomarenko, K. V. Vchivkov, W. Horton, 948 ¹²⁸Y. P. Zakharov, A. G. Ponomarenko, K. V. Vchivkov, W. Horton, 949 ¹²⁹Y. P. Zakharov, A. G. Ponomarenko, K. V. Vchivkov, W. Horton, 950 ¹³⁰Y. P. Zakharov, A. G. Ponomarenko, K. V. Vchivkov, W. Horton, 951 ¹³¹Y. P. Zakharov, A. G. Ponomarenko, K. V. Vchivkov, W. Horton, 952 ¹³²Y. P. Zakharov, A. G. Ponomarenko, K. V. Vchivkov, W. Horton, 953 ¹³³Y. P. Zakharov, A. G. Ponomarenko, K. V. Vchivkov, W. Horton, 954 ¹³⁴Y. P. Zakharov, A. G. Ponomarenko, K. V. Vchivkov, W. Horton, 955 ¹³⁵Y. P. Zakharov, A. G. Ponomarenko, K. V. Vchivkov, W. Horton, 956 ¹³⁶Y. P. Zakharov, A. G. Ponomarenko, K. V. Vchivkov, W. Horton, 957 ¹³⁷Y. P. Zakharov, A. G. Ponomarenko, K. V. Vchivkov, W. Horton, 958 ¹³⁸Y. P. Zakharov, A. G. Ponomarenko, K. V. Vchivkov, W. Horton, 959 ¹³⁹Y. P. Zakharov, A. G. Ponomarenko, K. V. Vchivkov, W. Horton, 960 ¹⁴⁰Y. P. Zakharov, A. G. Ponomarenko, K. V. Vchivkov, W. Horton, 961 ¹⁴¹Y. P. Zakharov, A. G. Ponomarenko, K. V. Vchivkov, W. Horton, 962 ¹⁴²Y. P. Zakharov, A. G. Ponomarenko, K. V. Vchivkov, W. Horton, 963 ¹⁴³Y. P. Zakharov, A. G. Ponomarenko, K. V. Vchivkov, W. Horton, 964 ¹⁴⁴Y. P. Zakharov, A. G. Ponomarenko, K. V. Vchivkov, W. Horton, 965 ¹⁴⁵Y. P. Zakharov, A. G. Ponomarenko, K. V. Vchivkov, W. Horton, 966 ¹⁴⁶Y. P. Zakharov, A. G. Ponomarenko, K. V. Vchivkov, W. Horton, 967 ¹⁴⁷Y. P. Zakharov, A. G. Ponomarenko, K. V. Vchivkov, W. Horton, 968 ¹⁴⁸Y. P. Zakharov, A. G. Ponomarenko, K. V. Vchivkov, W. Horton, 969 ¹⁴⁹Y. P. Zakharov, A. G. Ponomarenko, K. V. Vchivkov, W. Horton, 970 ¹⁵⁰Y. P. Zakharov, A. G. Ponomarenko, K. V. Vchivkov, W. Horton, 971 ¹⁵¹Y. P. Zakharov, A. G. Ponomarenko, K. V. Vchivkov, W. Horton, 972 ¹⁵²Y. P. Zakharov, A. G. Ponomarenko, K. V. Vchivkov, W. Horton, 973 ¹⁵³Y. P. Zakharov, A. G. Ponomarenko, K. V. Vchivkov, W. Horton, 974 ¹⁵⁴Y. P. Zakharov, A. G. Ponomarenko, K. V. Vchivkov, W. Horton, 975 ¹⁵⁵Y. P. Zakharov, A. G. Ponomarenko, K. V. Vchivkov, W. Horton, 976 ¹⁵⁶Y. P. Zakharov, A. G. Ponomarenko, K. V. Vchivkov, W. Horton, 977 ¹⁵⁷Y. P. Zakharov, A. G. Ponomarenko, K. V. Vchivkov, W. Horton, 978 ¹⁵⁸Y. P. Zakharov, A. G. Ponomarenko, K. V. Vchivkov, W. Horton, 979 ¹⁵⁹Y. P. Zakharov, A. G. Ponomarenko, K. V. Vchivkov, W. Horton, 980 ¹⁶⁰Y. P. Zakharov, A. G. Ponomarenko, K. V. Vchivkov, W. Horton, 981 ¹⁶¹Y. P. Zakharov, A. G. Ponomarenko, K. V. Vchivkov, W. Horton, 982 ¹⁶²Y. P. Zakharov, A. G. Ponomarenko, K. V. Vchivkov, W. Horton, 983 ¹⁶³Y. P. Zakharov, A. G. Ponomarenko, K. V. Vchivkov, W. Horton, 984 ¹⁶⁴Y. P. Zakharov, A. G. Ponomarenko, K. V. Vchivkov, W. Horton, 985 ¹⁶⁵Y. P. Zakharov, A. G. Ponomarenko, K. V. Vchivkov, W. Horton, 986 ¹⁶⁶Y. P. Zakharov, A. G. Ponomarenko, K. V. Vchivkov, W. Horton, 987 ¹⁶⁷Y. P. Zakharov, A. G. Ponomarenko, K. V. Vchivkov, W. Horton, 988 ¹⁶⁸Y. P. Zakharov, A. G. Ponomarenko, K. V. Vchivkov, W. Horton, 989 ¹⁶⁹Y. P. Zakharov, A. G. Ponomarenko, K. V. Vchivkov, W. Horton, 990 ¹⁷⁰Y. P. Zakharov, A. G. Ponomarenko, K. V. Vchivkov, W. Horton, 991 ¹⁷¹Y. P. Zakharov, A. G. Ponomarenko, K. V. Vchivkov, W. Horton, 992 ¹⁷²Y. P. Zakharov, A. G. Ponomarenko, K. V. Vchivkov, W. Horton, 993 ¹⁷³Y. P. Zakharov, A. G. Ponomarenko, K. V. Vchivkov, W. Horton, 994 ¹⁷⁴Y. P. Zakharov, A. G. Ponomarenko, K. V. Vchivkov, W. Horton, 995 ¹⁷⁵Y. P. Zakharov, A. G. Ponomarenko, K. V. Vchivkov, W. Horton, 996 ¹⁷⁶Y. P. Zakharov, A. G. Ponomarenko, K. V. Vchivkov, W. Horton, 997 ¹⁷⁷Y. P. Zakharov, A. G. Ponomarenko, K. V. Vchivkov, W. Horton, 998 ¹⁷⁸Y. P. Zakharov, A. G. Ponomarenko, K. V. Vchivkov, W. Horton, 999 ¹⁷⁹Y. P. Zakharov, A. G. Ponomarenko, K. V. Vchivkov, W. Horton, 999 ¹⁸⁰Y. P. Zakharov, A. G. Ponomarenko, K. V. Vchivkov, W. Horton, 999 ¹⁸¹Y. P. Zakharov, A. G. Ponomarenko, K. V. Vchivkov, W. Horton, 999 ¹⁸²Y. P. Zakharov, A. G. Ponomarenko, K. V. Vchivkov, W. Horton, 999 ¹⁸³Y. P. Zakharov, A. G. Ponomarenko, K. V. Vchivkov, W. Horton, 999 ¹⁸⁴Y. P. Zakharov, A. G. Ponomarenko, K. V. Vchivkov, W. Horton, 999 ¹⁸⁵Y. P. Zakharov, A. G. Ponomarenko, K. V. Vchivkov, W. Horton, 999 ¹⁸⁶Y. P. Zakharov, A. G. Ponomarenko, K. V. Vchivkov, W. Horton, 999 ¹⁸⁷Y. P. Zakharov, A. G. Ponomarenko, K. V. Vchivkov, W. Horton, 999 ¹⁸⁸Y. P. Zakharov, A. G. Ponomarenko, K. V. Vchivkov, W. Horton, 999 ¹⁸⁹Y. P. Zakharov, A. G. Ponomarenko, K. V. Vchivkov, W. Horton, 999 ¹⁹⁰Y. P. Zakharov, A. G. Ponomarenko, K. V. Vchivkov, W. Horton, 999 ¹⁹¹Y. P. Zakharov, A. G. Ponomarenko, K. V. Vchivkov, W. Horton, 999 ¹⁹²Y. P. Zakharov, A. G. Ponomarenko, K. V. Vchivkov, W. Horton, 999 ¹⁹³Y. P. Zakharov, A. G. Ponomarenko, K. V. Vchivkov, W. Horton, 999 ¹⁹⁴Y. P. Zakharov, A. G. Ponomarenko, K. V. Vchivkov, W. Horton, 999 ¹⁹⁵Y. P. Zakharov, A. G. Ponomarenko, K. V. Vchivkov, W. Horton, 999 ¹⁹⁶Y. P. Zakharov, A. G. Ponomarenko, K. V. Vchivkov, W. Horton, 999 ¹⁹⁷Y. P. Zakharov, A. G. Ponomarenko, K. V. Vchivkov, W. Horton, 999 ¹⁹⁸Y. P. Zakharov, A. G. Ponomarenko, K. V. Vchivkov, W. Horton, 999 ¹⁹⁹Y. P. Zakharov, A. G. Ponomarenko, K. V. Vchivkov, W. Horton, 999 ²⁰⁰Y. P. Zakharov, A. G. Ponomarenko, K. V. Vchivkov, W. Horton, 999 ²⁰¹Y. P. Zakharov, A. G. Ponomarenko, K. V. Vchivkov, W. Horton, 999 ²⁰²Y. P. Zakharov, A. G. Ponomarenko, K. V. Vchivkov, W. Horton, 999 ²⁰³Y. P. Zakharov, A. G. Ponomarenko, K. V. Vchivkov, W. Horton, 999 ²⁰⁴Y. P. Zakharov, A. G. Ponomarenko, K. V. Vchivkov, W. Horton, 999 ²⁰⁵Y. P. Zakharov, A. G. Ponomarenko, K. V. Vchivkov, W. Horton, 999 ²⁰⁶Y. P. Zakharov, A. G. Ponomarenko, K. V. Vchivkov, W. Horton, 999 ²⁰⁷Y. P. Zakharov, A. G. Ponomarenko, K. V. Vchivkov, W. Horton, 999 ²⁰⁸Y. P. Zakharov, A. G. Ponomarenko, K. V. Vchivkov, W. Horton, 999 ²⁰⁹Y. P. Zakharov, A. G. Ponomarenko, K. V. Vchivkov, W. Horton, 999 ²¹⁰Y. P. Zakharov, A. G. Ponomarenko, K. V. Vchivkov, W. Horton, 999 ²¹¹Y. P. Zakharov, A. G. Ponomarenko, K. V. Vchivkov, W. Horton, 999 ²¹²Y. P. Zakharov, A. G. Ponomarenko, K. V. Vchivkov, W. Horton, 999 ²¹³Y. P. Zakharov, A. G. Ponomarenko, K. V. Vchivkov, W. Horton, 999 ²¹⁴Y. P. Zakharov, A. G. Ponomarenko, K. V. Vchivkov, W. Horton, 999 ²¹⁵Y. P. Zakharov, A. G. Ponomarenko, K. V. Vchivkov, W. Horton, 999 ²¹⁶Y. P. Zakharov, A. G. Ponomarenko, K. V. Vchivkov, W. Horton, 999 ²¹⁷Y. P. Zakharov, A. G. Ponomarenko, K. V. Vchivkov, W. Horton, 999 ²¹⁸Y. P. Zakharov, A. G. Ponomarenko, K. V. Vchivkov, W. Horton, 999 ²¹⁹Y. P. Zakharov, A. G. Ponomarenko, K. V. Vchivkov, W. Horton, 999 ²²⁰Y. P. Zakharov, A. G. Ponomarenko, K. V. Vchivkov, W. Horton, 999 ²²¹Y. P. Zakharov, A. G. Ponomarenko, K. V. Vchivkov, W. Horton, 999 ²²²Y. P. Zakharov, A. G. Ponomarenko, K. V. Vchivkov, W. Horton, 999 ²²³Y. P. Zakharov, A. G. Ponomarenko, K. V. Vchivkov, W. Horton, 999 ²²⁴Y. P. Zakharov, A. G. Ponomarenko, K. V. Vchivkov, W. Horton, 999 ²²⁵Y. P. Zakharov, A. G. Ponomarenko, K. V. Vchivkov, W. Horton, 999 ²²⁶Y. P. Zakharov, A. G. Ponomarenko, K. V. Vchivkov, W. Horton, 999 ²²⁷Y. P. Zakharov, A. G. Ponomarenko, K. V. Vchivkov, W. Horton, 999 ²²⁸Y. P. Zakharov, A. G. Ponomarenko, K. V. Vchivkov, W. Horton, 999 ²²⁹Y. P. Zakharov, A. G. Ponomarenko, K. V. Vchivkov, W. Horton, 999 ²³⁰Y. P. Zakharov, A. G. Ponomarenko, K. V. Vchivkov, W. Horton, 999 ²³¹Y. P. Zakharov, A. G. Ponomarenko, K. V. Vchivkov, W. Horton, 999 ²³²Y. P. Zakharov, A. G. Ponomarenko, K. V. Vchivkov, W. Horton, 999 ²³³Y. P. Zakharov, A. G. Ponomarenko, K. V. Vchivkov, W. Horton, 999 ²³⁴Y. P. Zakharov, A. G. Ponomarenko, K. V. Vchivkov, W. Horton, 999 ²³⁵Y. P. Zakharov, A. G. Ponomarenko, K. V. Vchivkov, W. Horton, 999 ²³⁶Y. P. Zakharov, A. G. Ponomarenko, K. V. Vchivkov, W. Horton, 999 ²³⁷Y. P. Zakharov, A. G. Ponomarenko, K. V. Vchivkov, W. Horton, 999 ²³⁸Y. P. Zakharov, A. G. Ponomarenko, K. V. Vchivkov, W. Horton, 999 ²³⁹Y. P. Zakharov, A. G. Ponomarenko, K. V. Vchivkov, W. Horton, 999 ²⁴⁰Y. P. Zakharov, A. G. Ponomarenko, K. V. Vchivkov, W. Horton, 999 ²⁴¹Y. P. Zakharov, A. G. Ponomarenko, K. V. Vchivkov, W. Horton, 999 ²⁴²Y. P. Zakharov, A. G. Ponomarenko, K. V. Vchivkov, W. Horton, 999 ²⁴³Y. P. Zakharov, A. G. Ponomarenko, K. V. Vchivkov, W. Horton, 999 ²⁴⁴Y. P. Zakharov, A. G. Ponomarenko, K. V. Vchivkov, W. Horton, 999 ²⁴⁵Y. P. Zakharov, A. G. Ponomarenko, K. V. Vchivkov, W. Horton, 999 ²⁴⁶Y. P. Zakharov, A. G. Ponomarenko, K. V. Vchivkov, W. Horton, 999 ²⁴⁷Y. P. Zakharov, A. G. Ponomarenko, K. V. Vchivkov, W. Horton, 999 ²⁴⁸Y. P. Zakharov, A. G. Ponomarenko, K. V. Vchivkov, W. Horton, 999 ²⁴⁹Y. P. Zakharov, A. G. Ponomarenko, K. V. Vchivkov, W. Horton, 999 ²⁵⁰Y. P. Zakharov, A. G. Ponomarenko, K. V. Vchivkov, W. Horton, 999 ²⁵¹Y. P. Zakharov, A. G. Ponomarenko, K. V. Vchivkov, W. Horton, 999 ²⁵²Y. P. Zakharov, A. G. Ponomarenko, K. V. Vchivkov, W. Horton, 999 ²⁵³Y. P. Zakharov, A. G. Ponomarenko, K. V. Vchivkov, W. Horton, 999 ²⁵⁴Y. P. Zakharov, A. G. Ponomarenko, K. V. Vchivkov, W. Horton, 999 ²⁵⁵Y. P. Zakharov, A. G. Ponomarenko, K. V. Vchivkov, W. Horton, 999 ²⁵⁶Y. P. Zakharov, A. G. Ponomarenko, K. V. Vchivkov, W. Horton, 999 ²⁵⁷Y. P. Zakharov, A. G. Ponomarenko, K. V. Vchivkov, W. Horton, 999 ²⁵⁸Y. P. Zakharov, A. G. Ponomarenko, K. V. Vchivkov, W. Horton, 999 ²⁵⁹Y. P. Zakharov, A. G. Ponomarenko, K. V. Vchivkov, W. Horton, 999 ²⁶⁰Y. P. Zakharov, A. G. Ponomarenko, K. V. Vchivkov, W. Horton, 999 ²⁶¹Y. P. Zakharov, A. G. Ponomarenko, K. V. Vchivkov, W. Horton, 999 ²⁶²Y. P. Zakharov, A. G. Ponomarenko, K. V. Vchivkov, W. Horton, 999 ²⁶³Y. P. Zakharov, A. G. Ponomarenko, K. V. Vchivkov, W. Horton, 999 ²⁶⁴Y. P. Zakharov, A. G. Ponomarenko, K. V. Vchivkov, W. Horton, 999 ²⁶⁵Y. P. Zakharov, A. G. Ponomarenko, K. V. Vchivkov, W. Horton, 999 ²⁶⁶Y. P. Zakharov, A. G. Ponomarenko, K. V. Vchivkov, W. Horton, 999 ²⁶⁷Y. P. Zakharov, A. G. Ponomarenko, K. V. Vchivkov, W. Horton, 999 ²⁶⁸Y. P. Zakharov, A. G. Ponomarenko, K. V. Vchivkov, W. Horton, 999 ²⁶⁹Y. P. Zakharov, A. G. Ponomarenko, K. V. Vchivkov, W. Horton, 999 ²⁷⁰Y. P. Zakharov, A. G. Ponomarenko, K. V. Vchivkov, W. Horton, 999 ²⁷¹Y. P. Zakharov, A. G. Ponomarenko, K. V. Vchivkov, W. Horton, 999 ²⁷²Y. P. Zakharov, A. G. Ponomarenko, K. V. Vchivkov, W. Horton, 999 ²⁷³Y. P. Zakharov, A. G. Ponomarenko, K. V. Vchivkov, W. Horton*

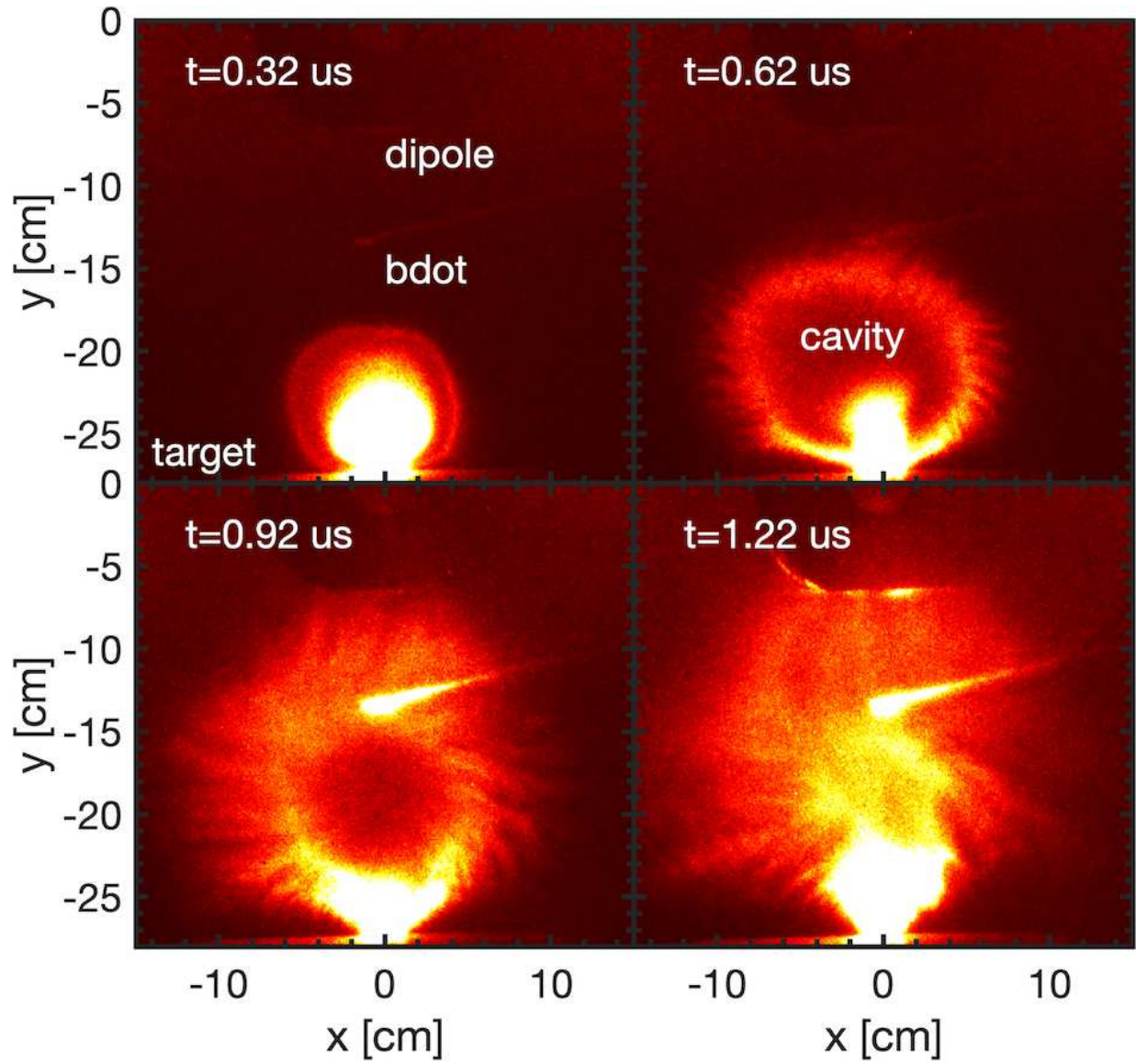
This is the author's peer reviewed, accepted manuscript. However, the online version of record will be different from this version once it has been copyedited and typeset.
PLEASE CITE THIS ARTICLE AS DOI: 10.1063/5.0084353



This is the author's peer reviewed, accepted manuscript. However, the online version of record will be different from this version once it has been copyedited and typeset.

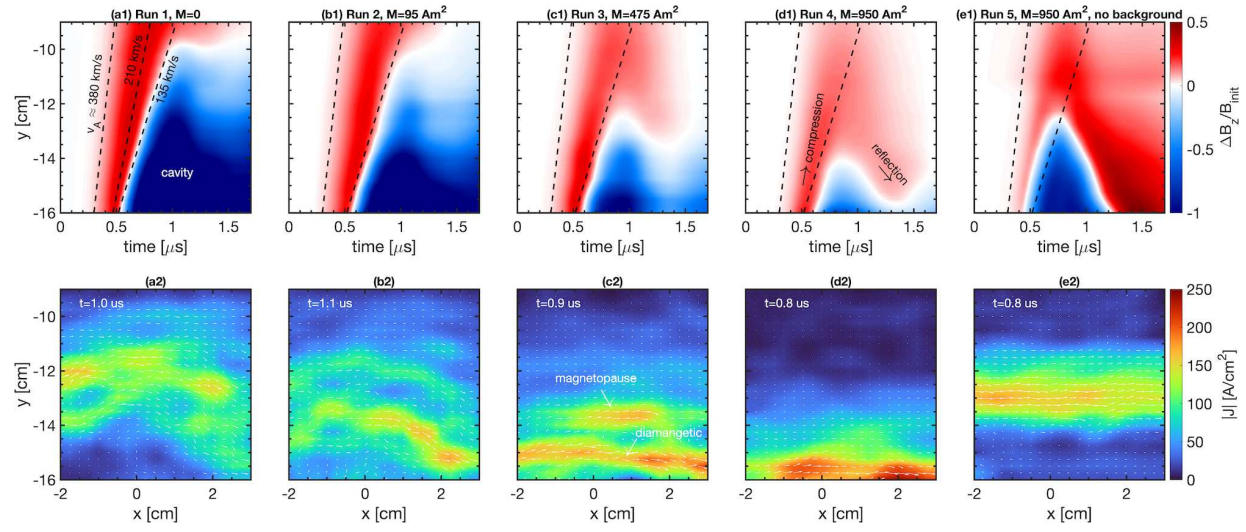
PLEASE CITE THIS ARTICLE AS DOI: 10.1063/5.0084353





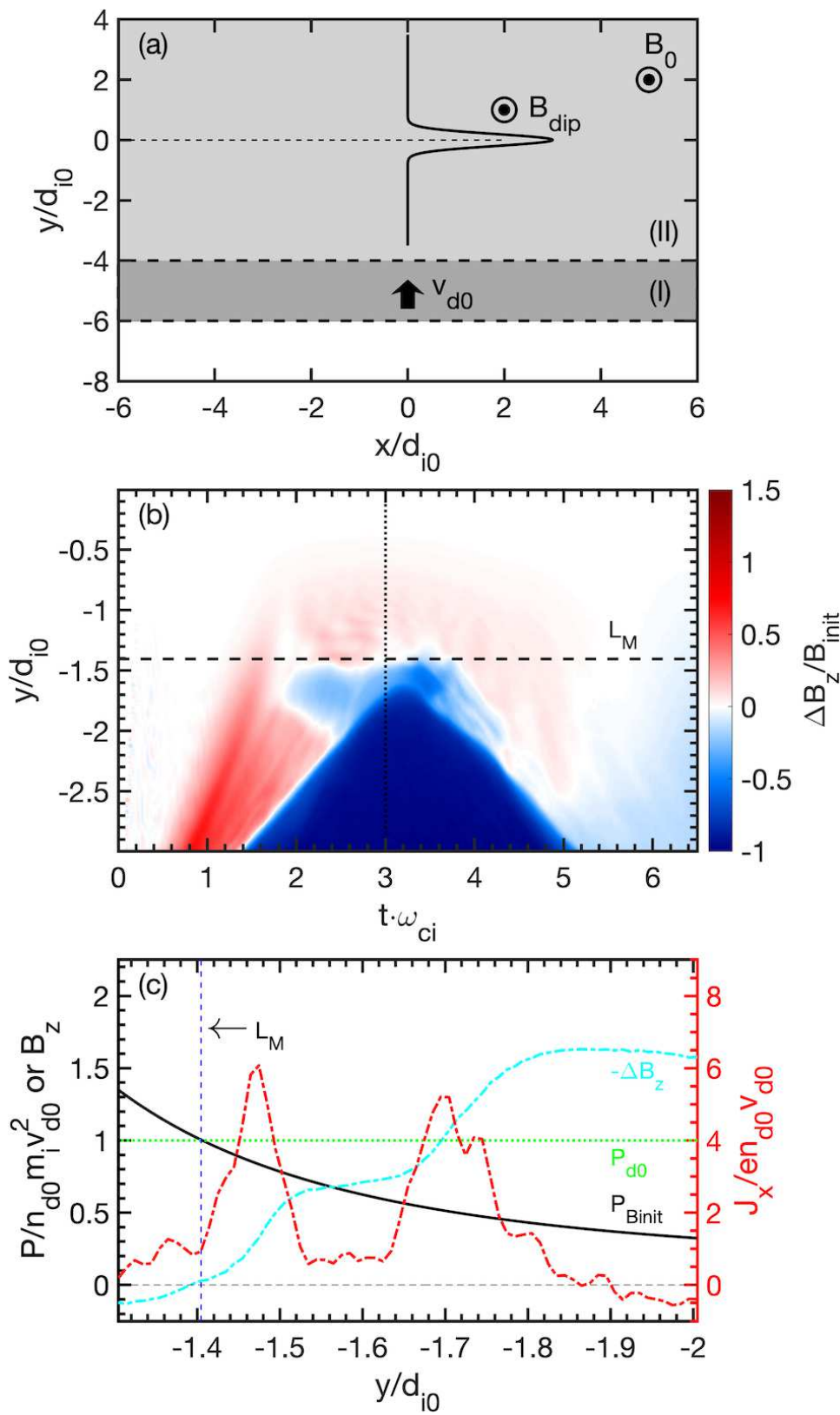
This is the author's peer reviewed, accepted manuscript. However, the online version of record will be different from this version once it has been copyedited and typeset.

PLEASE CITE THIS ARTICLE AS DOI: 10.1063/5.0084353



This is the author's peer reviewed, accepted manuscript. However, the online version of record will be different from this version once it has been copyedited and typeset.

PLEASE CITE THIS ARTICLE AS DOI: 10.1063/5.0084353



This is the author's peer reviewed, accepted manuscript. However, the online version of record will be different from this version once it has been copyedited and typeset.

PLEASE CITE THIS ARTICLE AS DOI: 10.1063/5.0084353

